NASA/CR—1999-209156

Active Control of Fan Noise by Vane Actuators

Alan R.D. Curtis
BBN Technologies, A Unit of GTE Internetworking, Cambridge, Massachusetts

Prepared under Contract NAS1–20101

National Aeronautics and
Space Administration

Glenn Research Center

May 1999

Trade names or manufacturers' names are used in this report for identification only. This usage does not constitute an official endorsement, either expressed or implied, by the National Aeronautics and Space Administration.

Available from

NASA Center for Aerospace Information
7121 Standard Drive
Hanover, MD 21076
Price Code: A05

National Technical Information Service
5285 Port Royal Road
Springfield, VA 22100
Price Code: A05

Summary

An active noise control system for ducted fan noise was built that uses actuators located in stator vanes. The actuators were piezoelectric benders manufactured using the THUNDER technology and were custom designed for the application.

The active noise control system was installed in the NASA ANCF rig. Four actuator arrays with a total of 168 actuators in 28 stator vanes were used.

Simultaneous reductions of acoustic power in both the inlet and exhaust duct were demonstrated for a fan disturbance that contained two radial mode orders in both inlet and exhaust. Total power levels in the target modes were reduced by up to 9 dB in the inlet and total tone levels by over 6 dB while exhaust power levels were reduced by up to 3 dB. Far field sound pressure level reductions of up to 17 dB were observed.

A simpler control system, matched to the location of the disturbance with two radial actuator arrays, was demonstrated to control total acoustic power in four disturbance modes simultaneously in inlet and exhaust.

The vane actuator met the requirements given for the ANCF, although in practice the performance of the system was limited by the constraints of the power amplifiers and the presence of control spillover. The vane actuators were robust. None of the 168 vane actuators failed during the tests.

Contents

List of Figures

List of Tables

Chapter 1

Introduction

One of the major sources of noise from the engines of modern commercial jet aircraft is the noise from the large fan at the front of the engine. High by-pass gas turbine engines derive most of their thrust from this fan which is driven by the turbine and pushes air though the by-pass duct around the engine core. The swirling motion of the air from the fan is straighten by fan exit guide vanes. An interaction between the flow from the fan and the stator vanes produces a characteristic tone known as fan/stator interaction noise. This tonal noise is a significant component of community noise metrics.

Control of fan/stator interaction noise is tackled either by modifying the source of the disturbance or by preventing transmission and radiation of the sound in and from the fan duct. Source control methods include measures such as selecting the number of fan blades and stator vane to ensure that only a few acoustic disturbance modes are generated, and modifying the geometry of the stator vanes through sweep and lean. Transmission control methods are predominantly the modification of the acoustic impedance of the lining of the fan duct wall to absorb or reflect the acoustic modes of the disturbance.

As the disturbance is tonal, active noise control has potential as a solution to fan-/stator interaction noise. Experimental investigations of active noise control have been transmission control methods; acoustic actuators mounted in the duct walls are used to reflect or absorb the modes of the disturbance [1, 2].

Vane actuators offer a method of applying active noise control at the source of the disturbance [3]. As both the unsteady forces of the fan wake passing over the vane, and the acoustic sources of the vane actuators are at the same location, then there is a potential efficiency benefit over active noise control systems that use actuators in the duct walls.

Analytical studies of the active control of fan noise using vane actuators [3, 4] have suggested that the technique may be feasible.

This report describes the development of an active noise control system that uses vane actuators and the demonstration of the system on the NASA Active Noise Control Fan installation at the NASA Lewis Research Center.

Chapter 2

Design of Vane Actuators

2.1 Requirements

The noise levels and environment in a commercial turbofan engine are severe, and in order to evaluate the feasibility of vane actuators for active noise control (ANC), United Technologies Research Center conducted an investigation of requirements and a study of potential actuator technologies [4]. This study concluded that, although active noise control of fan noise by vane actuators is feasible, no actuator available at the time met the requirements and that development of such actuators was required.

The requirements for the NASA Active Noise Control Fan (ANCF) are less severe but still demanding. The basic requirement is that the actuator must make enough noise; in order to be able to cancel the sound produced by fan/stator interaction, the ANC actuator must be capable of making at least the same level of sound. The actuator must also fit within the confines of the vane profile, and at least two actuators must be placed across the chord at a given radial location. This restricts the actuators to widths of approximately one inch and thicknesses of less than one quarter inch. There is more room in the spanwise dimension, an actuator length of 3 to 5 inches can be accommodated.

Estimates of the displacements required were available from a simulation of a flat plate cascade model of a vane set using a two dimensional fluid dynamics simulation code. For actuators of the size that can fit in the vane, displacements in excess of 25 μm rms would be required.

There are, of course, other engineering requirements including cost, reliability, power consumption, environmental requirements including temperature tolerance

and system integration considerations.

2.2 THUNDER: Introduction

THUNDER is an actuator technology invented at NASA Langley Research Center [11]. The acronym stands for THin UNimorph DrivEr and sensoR.

A THUNDER actuator is a composite of three thin layers, a metal base, a piezoelectric wafer and a metal top cover, bonded together under pressure and at high temperature with the LaRC SI polyimide adhesive. When a voltage is applied between the metal layers across the PZT it expands, and the differential in-plane stresses cause the actuator to bend or generate a force. The very high bond strength created by the use of the polyimide and the manufacturing process results in a very robust device that can be taken to high strains without fracture. The high displacement capability lead to some initial investigations into the feasibility of the use of THUNDER devices as vane actuators for the ANCF.

At the time of the investigation, no physical models of THUNDER actuators were available, and in order to understand the mechanism and properties of the devices, a series of models were constructed and experimentally verified. An understanding of the basic mechanisms allowed educated design of devices to meet a given specification. However, as was discovered early in the development process, the details of each physical device and in particular the method of fixing the device to a support have a great deal of variability that makes accurate prediction of performance problematic.

The pure boundary conditions of an analytical model are often difficult and impractical to implement and the actuator mounting is chosen to meet the mechanical requirements of the application while attempting to optimize one or more performance variables. For example, as a vane actuator the THUNDER actuator is to be used as a sound source and a mechanical requirement is that a good air seal is obtained from the front to the back of the actuator and that this seal does not fail or fatigue during operation. Good acoustic performance requires that the volume displacement of the actuator at the design frequency be optimized.

Another major practical effect is the static curvature caused by the thermal prestress which occurs both across the length and width. This shell curvature will stiffen the actuator leading to higher resonance frequencies and lower displacements. The actual curvature of an installed actuator is hard to accurately predict as it depends on both the details of the mounting and the manufacturing process of the actuator. Small variations in each can lead to large variations in resonance frequency.

Thus while the models developed are useful for understanding the relationship between design variables (material choices and dimensions) and performance variables (force and displacement per volt or ampere), they were used only provide approximate predictions of actual performance. In order to optimize the design for the ANCF, a number of prototype devices and mounting schemes were experimentally investigated.

2.3 THUNDER Models

Three different models were developed to aid the design of the THUNDER actuators.

The first was a simple analytical model that gave insight into the physical mechanisms of the actuation process and provided design guidance as to what variables to adjust to optimize device performance. This model was based on a layered two dimensional beam structure.

The effects of the third dimension, and in particular the stiffening effect of the curvature induced by thermal pre-stress were investigated using the second model. BBN SARA, a Finite Element Method program for structural acoustics was used to verify the results of the analytical model and to predict the behavior of actuators with shell curvature.

When experimentally investigating prototype actuators, a third model was used. This equivalent circuit model generated simple measurable quantities that allowed comparison of measured transducer parameters between designs.

2.4 Design Approximations

The simple two dimensional beam structure analytical model was used to develop some design approximations and guidelines, allowing the dependence of such quantities as the displacement per volt and the first natural frequency of the device on design variables such as material choices and layer thicknesses.

In general, a thinner PZT results in greater actuator displacement at the expense of greater actuator force, and for an acoustic actuator, the thinnest PZT material available should be selected. The thickness of available PZT wafers is determined both by the manufacturing process of the wafer itself and by the need to handle the wafer for subsequent processing (as a ceramic PZT is fragile and fractures easily). The thickness of the PZT chosen for incorporation into a THUNDER device is thus

likely to be fixed by its availability. At the time of this investigation, the thinnest PZT readily available was approximately 175 μm thick.

However, an important design parameter that can have a large impact on performance is the selection of the base layer. As a rule of thumb, maximum displacement occurs when

$$Y_a h_a = Y_b h_b$$

where Y_a is the modulus of the base layer, h_a is the thickness of the base layer, Y_b is the modulus of the PZT layer, and h_b is the thickness of the PZT layer. All subsequent approximations make the assumption that the base layer has been selected such that this design criterion has been met. For PZT around 175 μm thick, a metal base layer of between 125-250 μm is typical.

Some useful basic approximations are those for the bending stiffness B

$$B \approx \frac{Y_b h_b^3}{3}$$

and the piezoelectric bending moment M_p.

$$M_p \approx \frac{h_b^2}{3} Y_b d_{31} E_3$$

E_3 is the applied electrical field and d_{31} is the piezoelectric constant for the material. The resulting curvature caused by an applied electric field will be the ratio of moment to bending stiffness.

$$c \approx -\frac{d_{31} E_3}{h_b}$$

The displacement output is related to the curvature by

$$u_0 = c\Phi_0$$

where Φ_0 is $l^2/8$ for a simply supported actuator.

Having selected the PZT and base layer thicknesses, the next step is to choose the length of the actuator. The displacement output increases with the square of the length of the actuator and so longer actuators are preferred. However, the first resonance frequency of the actuator is inversely proportional to the square of the length of the actuator and, in general we will want to operate the actuator at frequencies below the resonance. At and near the resonance, although the increased output is attractive, the performance of the actuator is unpredictable and the phase shift accompanying the resonance makes the actuator difficult to control. The design choice is then to make the actuator as long as possible such that the operating bandwidth of the actuator falls below the first resonance.

The first resonance frequency can be approximated by

$$\omega_1 = \frac{\beta}{l^2}\sqrt{\frac{B}{\rho_i h_i}} \approx \frac{\beta}{\sqrt{3}}\frac{h_b}{l^2}\sqrt{\frac{Y_b}{\rho_b}}$$

where the constant β depends on the choice of boundary conditions and is approximately 10 for a simply supported device. The stiffness and thus resonance frequency of the actuator will, in practice, depend on the specific details of both the mounting and the static curvature induced by the thermal pre-stress.

If ω_0 is the greatest frequency at which the actuator will be operated, then we require that

$$\omega_0 \leq \omega_1$$

Thus the length of the actuator is given by

$$l^2 \leq \frac{\beta h_b}{\sqrt{3}\omega_0}\sqrt{\frac{Y_b}{\rho_b}}$$

and the maximum displacement

$$u_{\max} \propto cl^2 \propto d_{31}E_3\frac{\beta}{\omega_0}\sqrt{\frac{Y_b}{\rho_b}}$$

2.5 Equivalent Circuit Model

When designing a THUNDER actuator for a particular application, it is useful to have a transducer model that relates the electrical input power variables voltage and current to the mechanical input power variables force and velocity using parameters that can be experimentally measured and hence allow candidate designs to be compared. A useful tool for this purpose is the equivalent electrical circuit shown in figure 2.1.

In the center of the diagram is an ideal transformer with a 'turns ratio' of N. N is the key transduction constant that relates input current to velocity (or charge to displacement). Turning the circuit around would give the sensor relationships of volts per force and charge per displacement. C_e represents the electrical capacitance for the stress free actuator. C_m represents the mechanical compliance for a open circuit actuator

The approximations for the circuit parameters are

$$N \approx \frac{\Phi_0 d_{31}}{A h_b e_{33}} = \frac{\Phi_0 g_{31}}{A h_b}$$

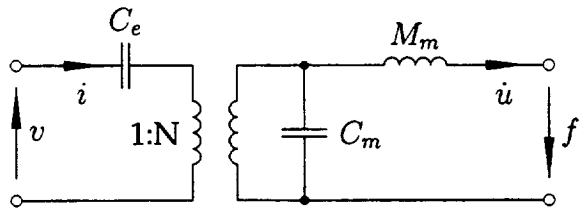

Figure 2.1: An equivalent circuit for a THUNDER actuator

The ratio d_{31}/e_{33} is the g_{31} constant for the PZT material.

$$C_e = \frac{Ae_{33}}{h_b}$$

$$NC_e = \frac{\Phi_0 d_{31}}{h_b^2}$$

and

$$NC_e/C_m = \frac{Y_b h_b A d_{31}}{3\Phi_0}$$

2.6 Thermally Induced Curvature

In the THUNDER manufacturing process, a thermal pre-stress is caused by the different amounts that the constituent layers shrink due to their different coefficients of thermal expansion. The adhesive between layers sets at a high temperature and as the actuator cools, the metal layers shrink more than the PZT. The PZT layer is put into compression while the metal layers are in tension. This causes the actuator to bend.

It is possible to estimate the curvature for a given actuator and manufacturing process. However, accuracy is difficult as the eventual curvature depends on the bending stiffness which in turn depends on the curvature (resulting in a cubic equation for bending stiffness) and also the precise details of the mounting of the actuator,

An approximation for the thermal bending moment is

$$M_\theta = Y_b h_b^2 (\alpha_a - \alpha_b)\theta/3$$

where α_a and α_b are the coefficients of thermal expansion for the base and PZT layers and θ is the temperature (above ambient) at which the actuator adhesive set

(250 degrees Celcius for LaRC-SI). A first pass estimate of the curvature would then be

$$c = M_\theta / B = (\alpha_a - \alpha_b)\theta / h_b$$

If the curvature is large then the actuator will be stiffer than predicted by a factor x where

$$x \approx \left(\frac{l^2(\alpha_a - \alpha_b)\theta}{h_b^3 \beta} \right)^{2/3} \tag{2.1}$$

The bending stiffness B and the stiffness K must be increased and the compliance C_m must be decreased by this factor.

2.7 Prototype Testing

A series of actuator prototypes of varying design were built and tested to gain an understanding of the dependency of design variables and to develop a practical method of construction. A number of design issues were confronted during this process.

An early decision was to design the actuators to have a resonant frequency above the nominal operating frequency of 1000 Hz. Although an actuator run at resonance can have an order of magnitude greater displacement than a non-resonant actuator, a system of resonant actuators is very difficult to control. In batch variability and interaction with a common structure results in actuators having slightly different resonant frequencies and hence displacement outputs. When used in a matched array, variability in actuator sensitivity translates into control spillover, reducing the effective noise reduction performance of the system. In addition, the rapid phase shifts that occur in the device transfer function at the resonance, can cause instability in the control system.

Running the actuators at resonance was considered inadvisable. As actuator batch variability lead to very different sensitivities above the first resonance, it was decided to run the actuators below their first resonance. However, as displacement output is inversely proportional to resonance frequency for an actuator of a given length, the resonant frequency should not be too far above the nominal operational frequency. Placing the resonance just above the operating frequency also allows for some benefit from the shoulder of resonant amplification without paying the price of running too close to resonance. For the operational frequency of 1000 Hz, its was decided to target an actuator resonance frequency of approximately 1200 Hz.

The most important design parameter was found to be the method of fixing the actuator to its support. As an acoustic actuator, the device requires an air tight seal between its front and rear sides and so is constrained on four edges. For a fixed length and natural frequency, a simply supported actuator produces more volume displacement than other boundary conditions. Attempts were made to engineer a simple support that allowed free rotation of the actuator while preventing in-plane motion at the support. This proved to be a challenge, but the final design produced actuators with a variation in resonance frequency of about 10 percent.

A second design issue was that of the thermal response of the actuators. When PZT is driven at high voltage levels, internal losses cause the material to heat. As the capacitance of PZT increases with temperature, a hotter device draws more current and so gets hotter still. With some device designs there is a potential problem of thermal feedback instability. At a certain drive level the increasing capacitance and increasing current heats the actuator to its Curie temperature at which the PZT material looses its piezoelectric properties and ceases to strain.

Although the ANCF vane actuators are cooled somewhat by the flow of air over the vane, the materials in the actuators were selected to minimize the sensitivity to thermal effects. A combination of PZT-5A piezoelectric and Beryllium Copper base metal was found to give the best trade-off between thermal sensitivity and displacement performance.

The drive level dependent properties of the PZT material was also apparent when the actuator sensitivity in displacement per volt was examined. Figure 2.2 illustrates this behavior for a prototype actuator close to the final design. At high drive levels this actuator exceeds the design requirement of 25 μm rms displacement at 1000 Hz. However, although at low levels the resonance frequency is above 1200 Hz, at high drive levels it has dropped to close to 1100 Hz. Although the increase in displacement due to the presence of the resonance is welcome (as long as all actuators in an array shift up by the same amount), the frequency shift has added approximately 45 degrees of phase to the frequency response function. This added phase could cause instability if it is unmodeled by the controller.

This frequency shift behavior can be partly explained by the drive dependent capacitance of the PZT material. This behavior can be seen in measurements of actuator dynamic capacitance; that is the measured transfer function between actuator voltage and charge. Figure 2.3 shows the dynamic capacitance for a prototype actuator driven at 10 V rms and 100 V rms. The capacitance at 1000 Hz doubles from around 70 nF to 140 nF.

The capacitance non-linearity also affects the actuator sensitivity expressed in displacement per volt. Figure 2.4 shows a graph of displacement output versus voltage drive level for the same prototype actuator driven at 1000 Hz; the displace-

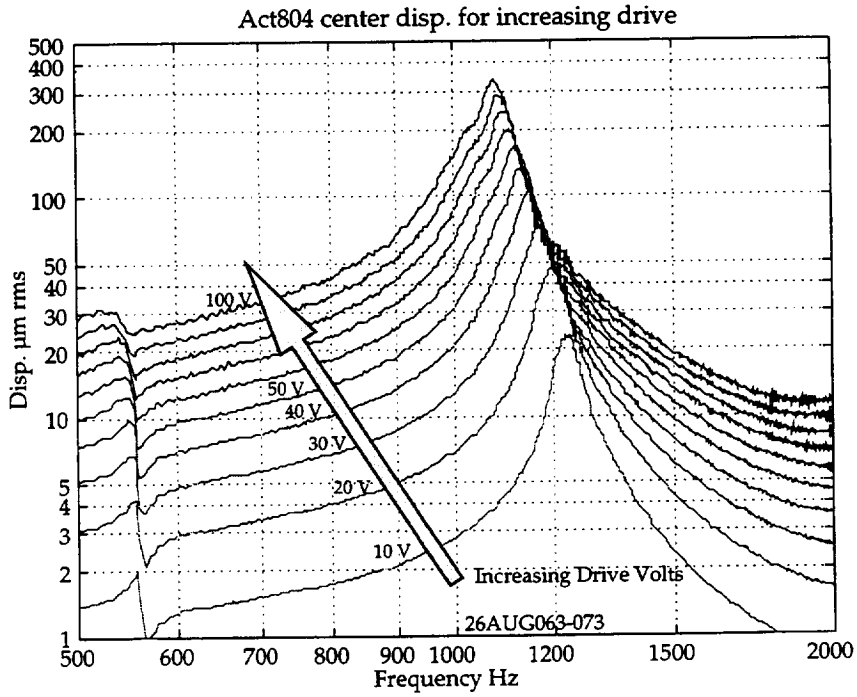

Figure 2.2: Actuator displacement vs. drive level.
The variation in actuator displacement output with increasing voltage drive level.
Note the decrease in resonance frequency with increasing drive level.

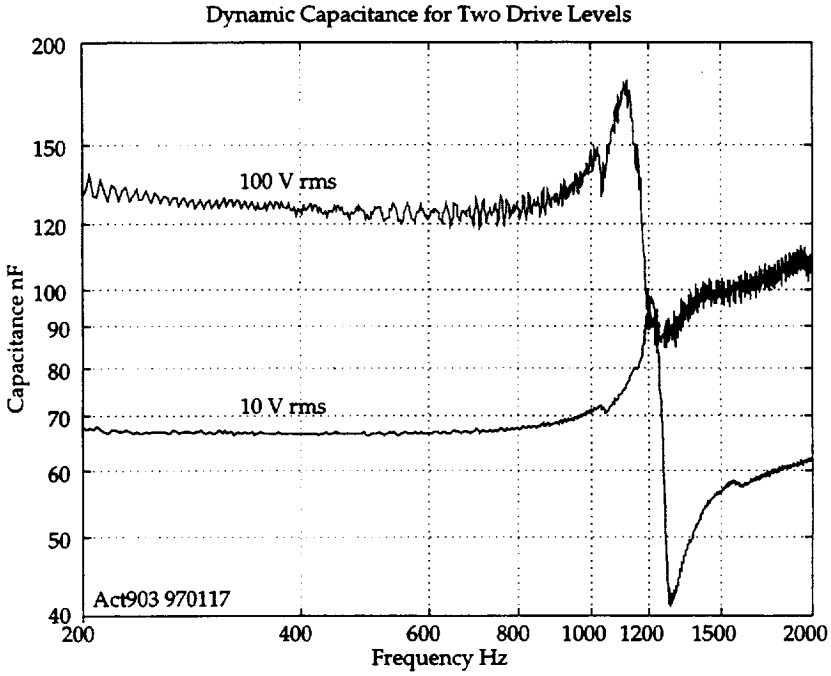

Figure 2.3: Actuator dynamic capacitance
Measured dynamic capacitance for a prototype actuator at low and high drive levels at 1000 Hz.

ment/voltage sensitivity increases with drive level as the resonance frequency drifts down towards the drive frequency.

However, PZT is a charge device, an applied charge causes a strain. The piezoelectric parameters expressed in terms of displacement/charge are less sensitive to drive level. The lower plot in Figure 2.4 shows a graph of displacement output versus current drive level; the displacement/current sensitivity is approximately uniform with drive level.

Experimental testing of prototype actuators produced two final candidates for the ANCF actuator. These similar designs both had resonance frequencies at about 1200 Hz and met the displacement requirements. They differed only in the choice of metal base thickness and top cover design. THUNDER actuators can have an optional top cover of thin metal foil, usually aluminum. This layer increases the compressive pre-stress in the PZT and provides a robust surface electrode. However, it also increases the bending stiffness and slightly reduces the actuator sensitivity. A set of actuators sufficient for four vanes was built, with half the actuators from each design. The four vanes were installed in the ANCF for a series of tests that were designed to quantify the control authority of the actuator arrays and to confirm that the specification derived from simulation was sufficient to cancel the fan/stator disturbance modes.

During these test the actuators with a top cover performed more reliably than the actuators without a top cover. The latter actuators exhibited calibration drift during the course of the experiments and at least one actuator suffered a failure. The calibration of the actuators with a top cover held their calibration well and none of them failed. The top cover design was selected for the full twenty eight vane tests.

2.8 Final Actuator Design

The final actuator design is illustrated in Figure 2.5. Three PZT-5A tiles each one inch long, 0.6 inches wide and 0.007 inches thick are bonded to a Beryllium Copper base 1.5 inches wide, 2.5 inches long and 0.005 inches thick. Not shown in the figure are the aluminum top covers for each tile. These were 0.001 inch thick and were trimmed to leave a small border at each edge of the tile.

The design of three tiles in one unit was chosen to select the required resonance frequency of 1200 Hz. For the mounting method used, actuators with this geometry have the required resonance for a length of about 1.1 inches, which was a convenient chordwise dimension for an ANCF vane actuator. Experimental experience suggested that actuators with a width to length aspect ratio of 0.6:1 performed well, other aspect ratios either had too much thermal pre-stress curvature or had less re-

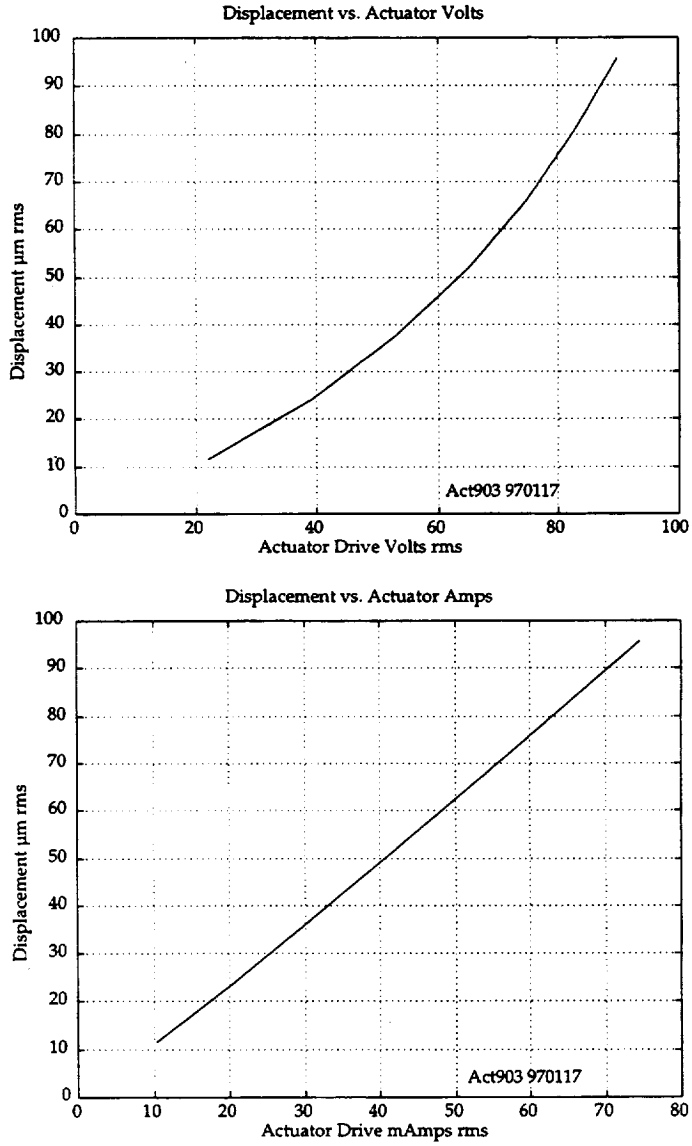

Figure 2.4: Actuator output linearity
Output sensitivity of a prototype actuator driven at 1000 Hz for different input drive levels. The upper plot is for a voltage input, the lower for a current input.

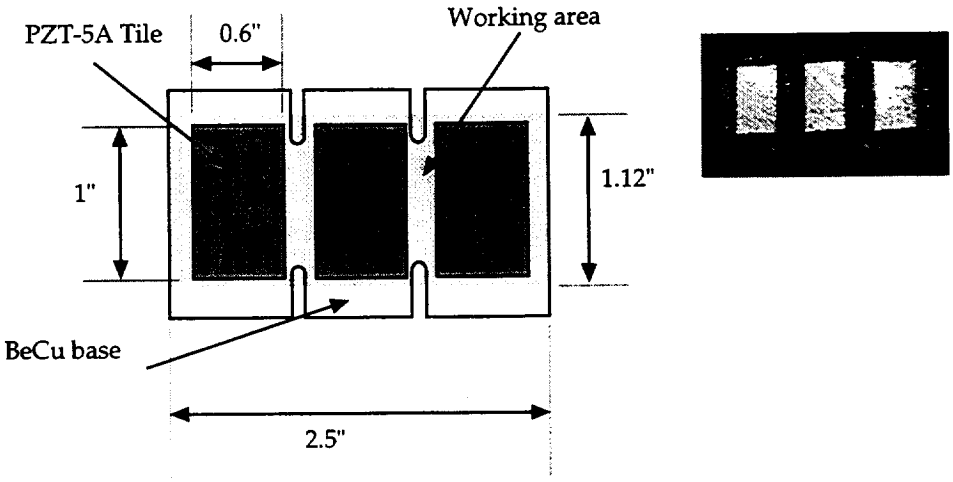

Figure 2.5: Actuator final design
The final design of the vane actuator for the ANCF test. The insert is a photograph of an uninstalled actuator.

peatable dynamic characteristics. The three tile design was a method of combining three individual actuators with the right dynamic characteristics to produce one device of the width required for the vane. The small slots in the long sides of the actuator are to relieve the thermal pre-stress curvature in the long dimension.

Figure 2.6 shows a typical response of the actuator for a 100 V rms drive level. The displacement is greater than 25 μm rms at 1000 Hz and the resonance frequency is at about 1200 Hz as required. The sound pressure output was measured at a level of 90 dB SPL for a 1 kHz sine wave at 1 m in an anechoic chamber. The total harmonic distortion was less than 26 dB; it is assumed that most of that distortion was due to the power electronics and not non-linearities in the actuator.

Figure 2.7 illustrates the installation of the actuators in the vane. A cross section of the vane is shown. The actuator inserted in a pocket machined in the vane and is bonded to a small retaining shelf. The actuator operates in dipole mode, radiating sound to both pressure and suction surfaces of the vane. The continuity of airflow over the vane is maintained on each surface by a cover sheet made from perforated metal that is bonded to the vane so that it conforms with the airfoil profile and lies flush with the surface. Figure 2.8 is a photograph of actuators installed in a vane.

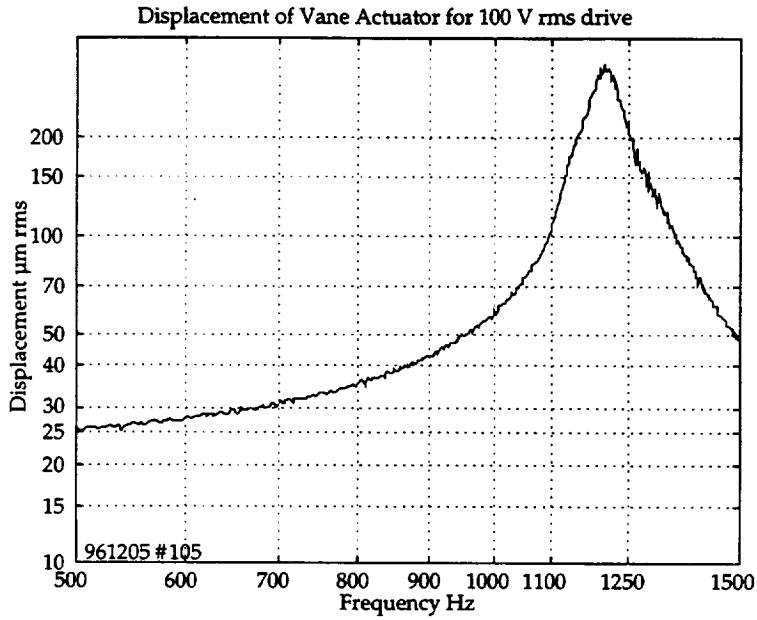

Figure 2.6: Actuator displacement response
A typical displacement response of the final actuator design.

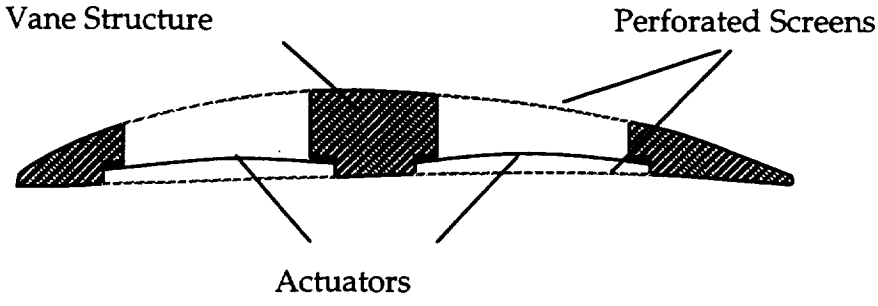

Figure 2.7: Actuator installation in vane
A cross section of a vane showing the installation of the actuators.

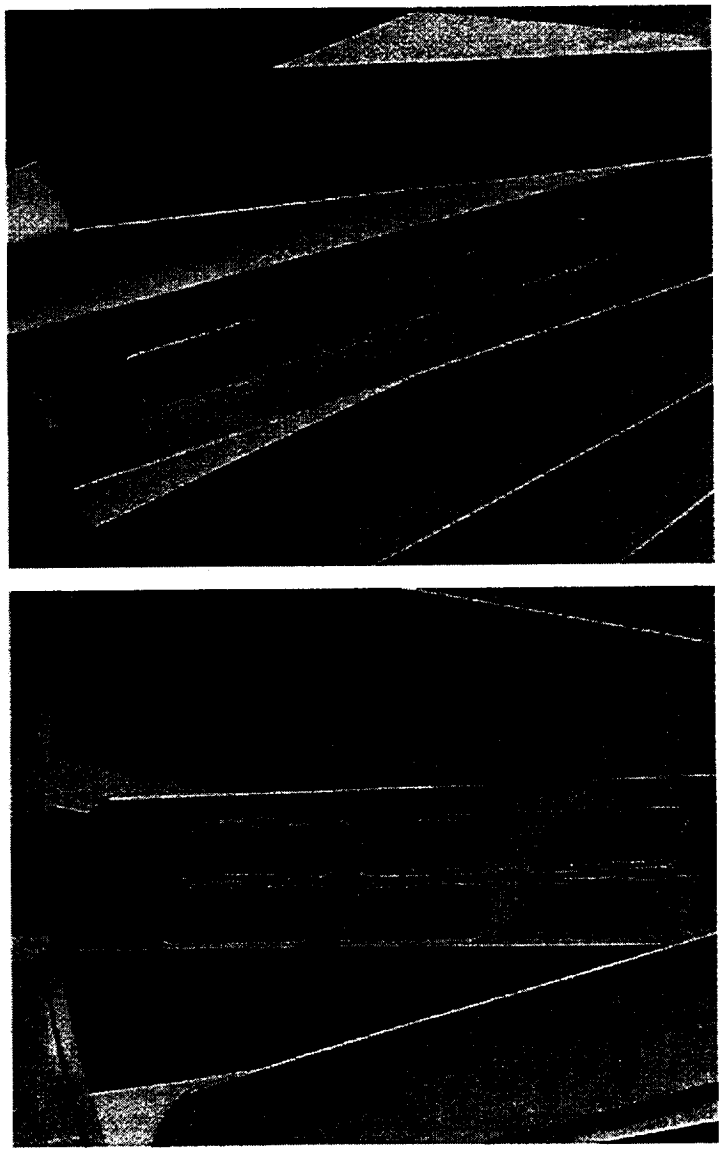

Figure 2.8: Photograph of a vane with installed actuators
A photograph of a vane with installed actuators from the four vane test. The suction side is shown at the top. The pressure side is shown at the bottom. The small red lines on the pressure side are the power leads to the actuators.

2.9 Selection of Actuator Location

The objective of the ANCF test was to cancel the disturbance sound simultaneously in both inlet and exhaust. It is it is not sufficient for the actuators to capable of producing the required level of sound, they must be capable of creating the correct mix of modes with the correct phase relationship. It is the phase relationship that is most difficult to meet, the required actuator outputs may be much larger for a mix of modes with a given phase than the same amplitude of modes with arbitrary phase.

As there are four acoustic modes in the disturbance, four vane actuators are required for cancellation. The displacement requirements of the actuators depends on their locations in the vane. In an effort in parallel to the actuator development, Ed Envia of NYMA studied the effect on actuator location in simulation, and provided guidance on the final location of the actuators.

The study used a simulation program called VO72 [5]. This is a three-dimensional rotor-stator interaction noise code which accommodates realistic annular geometries. The code couples a description of the unsteady aerodynamic interaction between the rotor wakes and stator vanes, to the three-dimensional acoustic response of a cascade in an annular duct containing a uniformly moving medium.

The source of noise is the harmonic surface pressure loading on the surface of the vane caused by the fan wake, in particular the the wake component normal to the vane surface, the stator upwash. Wakes are modeled as frozen gusts that are convected by the mean flow, which is assumed to be a function of the radius. The stator vane geometry is also simplified by assuming that vanes are infinitesimally thin flat surfaces. The rotor-stator noise field is computed by a surface integral of the vane pressure source terms combined with a suitable Green's function representation of the sound field in the duct including the effects of mean flow. A wake model and Green's functions derived for the ANCF were used to produce a set of complex disturbance mode amplitudes in inlet and exhaust that matched those measured in the rig.

Additional source terms representing the vane actuators were added to the model. The actuators were modeled as rectangular patches simply supported on four sides with a sinusoidal velocity distribution. These dipole sources were introduced one at a time and used to predict complex transfer functions between the patch velocity and the resulting mode amplitudes. By inverting the matrix of transfer functions, the required patch displacements were be calculated.

The simulation was run a number of times with different patch sizes and locations. The size and location of patches were constrained by the practical limitations of

the ANCF vane and the prototype vane actuators. In order to cancel both inlet and exhaust modes, two different chord-wise locations are required and the geometry of the vane limited the width of the actuators to about one inch. Wider actuators than this were found to be less effective. Optimal locations for the chordwise pair were as far apart as possible with one close to the leading edge and the other close to the trailing edge.

For each chordwise location, a pair of spanwise patches were used. These were initially matched to the radial distribution of the disturbance modes. A shorter tip actuator was used to avoid crossing the node of the first radial mode. A longer hub actuator was used. Optimal designs tended to make the tip actuator about 2.5 inches long and the hub actuator 5 inches long. For practical reasons, it was desired to have a single actuator design, and so the hub actuator was split into two 2.5 inch devices driven with the same velocity and separated by a suitable gap for the mounting structure. Within these constraints the radial location of the four actuators were varied and a solution with the least maximum displacement required to cancel the disturbance was retained.

2.10 Amplifier Design

As the displacement/current sensitivity of the actuators was more linear than the displacement/voltage sensitivity, it was decided that the power amplifiers should be current drive devices, providing a linear constant current proportional to the input signal, independent of the varying capacitance of the load. The amplifier design requirements were to deliver a drive voltage of 100 V rms at 1 kHz into a 140 nF load.

A schematic diagram of the amplifiers built for the ANCF test is shown in figure 2.9. The design is based on an APEX Model PA85 power operational amplifier. A feedback loop around the op-amp controls the current delivered. The output current is sensed by the voltage developed across the 5W resistor. This voltage is fed to a differential amplifier, Burr Brown Model INA117, which features high common mode rejection. A phase lag network, (R15,R13,C7) is added to the feedback path to assure stability. The output resistor R19 establishes the low frequency gain at 3000. The maximum current is set by the 3.9W resistor and the 68 pF plus 100W provide amplifier phase compensation. The amplifier was powered from a $\pm$ 160 Volt unregulated supply together with a $\pm$ 15 Volt supply to the INA117.

The mechanical packaging unit consisted of two amplifiers mounted to a common heatsink with forced air cooling. An assembly of four units occupied one 19 inch rack width. At maximum output, driving a 50 nF load at 1 kHz, each amplifier

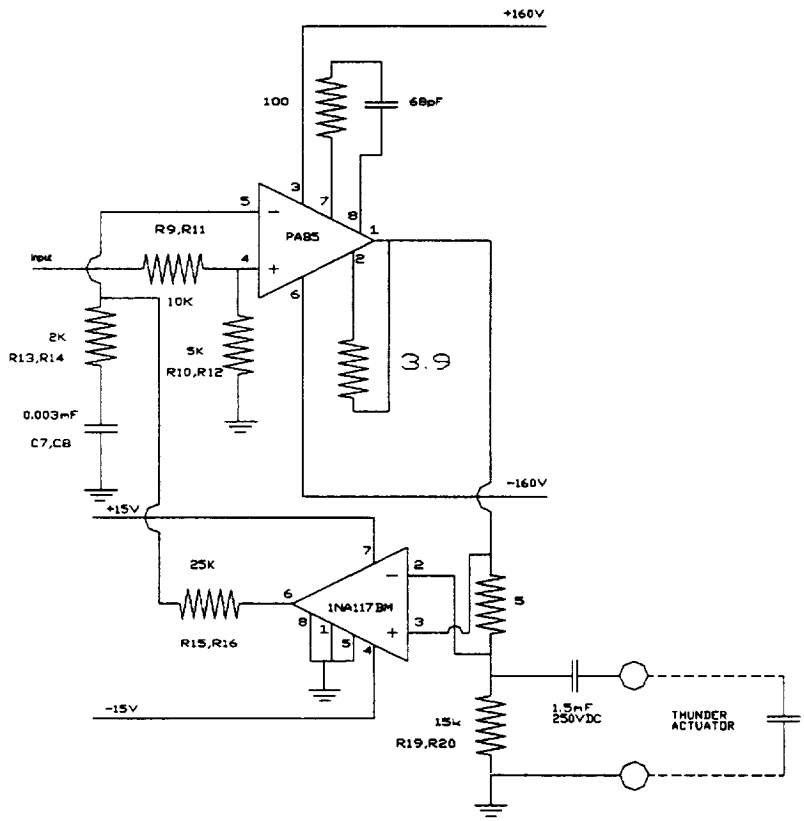

Figure 2.9: Schematic of amplifier design

channel dissipated 25 Watts.

The calculated voltage gain across the amplifier from which it will be observed that a constant current characteristic is produced between 200 and 1000 Hz.

The maximum drive signal is dependent on the load capacitance. The output voltage on a typical channel can be monitored from the front panel to ensure that the waveform does not clip. This would lead to higher than normal power dissipation in the output amplifier. The maximum available voltage is 140V.

The nominal sensitivity on all channels at max gain is 70 mA /Volt in. The amplifier has output current limiting at a nominal 200 mA

Example:- with 150 nF capacity, at 1 kHz, the load reactance is 1060W. At 140V output, the load current would be 132 mA. The input voltage to generate this current would be 1.89 V or 0.667 V rms.

Figure 2.10 shows the amplifier output voltage and current when attached to a typical pair of vane actuators.

2.11 Calibration

In order to prevent control modal spillover, each actuator in an array should have the same sensitivity. Most of the variability in actuator output was reduced by design of the mounting system and in careful control of the manufacturing process. However, as is inevitable, some variation remained.

There were two methods of calibrating installed actuators. Voltage/current ratios were taken as the primary sensitivity measure. A front panel switch on each amplifier rack enabled the monitoring of the voltage and current supplier to the pair of actuators attached to each amplifier channel. The gain of the amplifier from voltage in to current out was trimmed by a potentiometer on the front panel to ensure that each actuator pair in an array received the same current for the same drive signal.

As a pair of actuators were connected in parallel to the output of each amplifier channel, it was not possible to calibrate the current to individual actuators by this method. It was impractical to put a trimming potentiometer in the high voltage output side of the power amplifier and so a method of trimming the current sensitivity with a series capacitor was developed. A high voltage breakout circuit board was designed to be placed between the power amplifier output and the signal distribution vane grid that would allow the insertion of series capacitors in one of the paths to a pair of actuators. The capacitor would be selected to reduce the effective capacitance of the path with the highest capacitance to that of the lowest

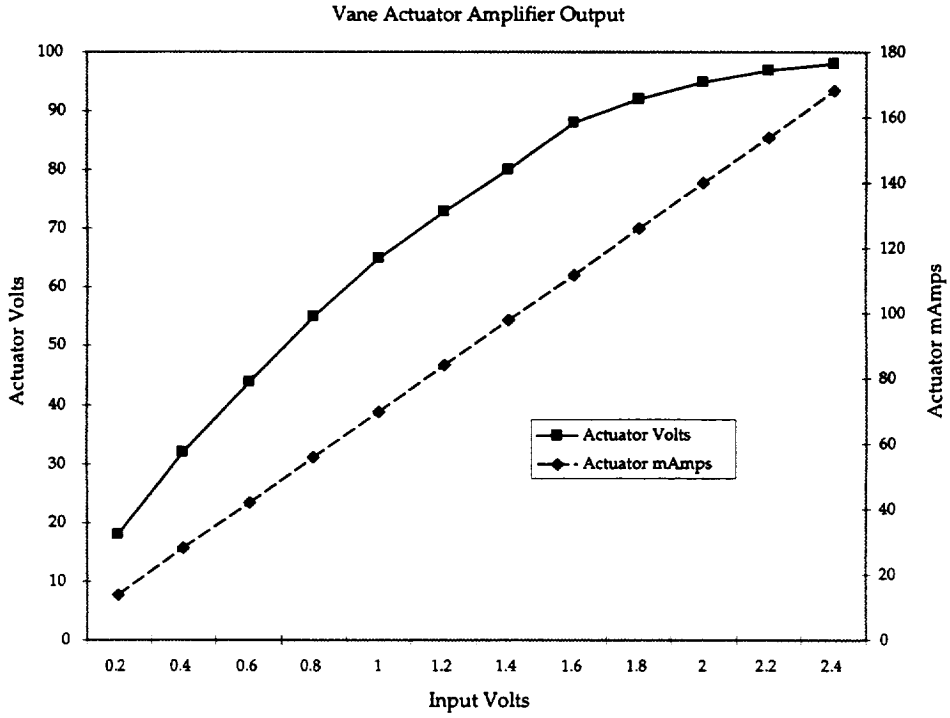

Figure 2.10: Amplifier linearity
The output voltage and current for the power amplifier attached to a typical pair of vane actuators

capacitance.

Displacement/current sensitivity is only an indication of the true sensitivity of concern, that between controller output voltage and the acoustic output of an actuator. An acoustic cavity calibrator was designed, with six microphones in six sealed cavities that could be fixed to the vane. Due to the level dependent sensitivity of the actuators, it is necessary to calibrate the actuators at close to full output power and, although this method allowed an approximate calibration to be performed, acoustic cross-talk between actuators was significant and proved to be sensitive to vane location. A better method would be required if a more accurate calibration is desired. Fortunately, control spillover was low enough for the system to demonstrate reasonable noise reduction levels.

One issue with both the front panel trimming potentiometer and the series trim capacitor is that they limit the maximum output of the actuators. The power amplifier output is primarily constrained by the maximum voltage swing of the operational amplifiers. In array of twenty eight actuators, this means that in order to calibrate the array, all channels have to be reduced to the sensitivity of the actuator with the smallest sensitivity. The maximum output of the array is constrained to the maximum output of the weakest actuator.

Chapter 3

Control System

3.1 Background Theory

The sound field of fan/stator interaction noise is usually represented by a set of spinning acoustic modes in the fan duct [6].

$$p(r,\theta,x,t) = \sum_{mn} A_{mn}(r) \exp j(\omega t - m\theta - k_x x) \tag{3.1}$$

The sound pressure at a location given in the cylindrical coordinates r, θ, x is the sum of terms with the complex amplitude $A_{mn}(r)$, a function of the radial location r, and a propagation term $\exp j(\omega t - m\theta - k_x x)$ which describes a spinning pattern with wavefronts that propagate with an axial phase velocity ω/k_x and simultaneously rotate with angular phase velocity ω/m. m is an integer, the circumferential mode order, that specifies the number of complete wavelengths around the circumference at any given axial location. For each m order, there are multiple radial patterns that each propagate with a different axial wavenumber k_x. Each radial pattern is distinguish by the number of nodal circles n, the radial mode order. The important properties of a given spinning mode are given in Table 3.1

The first mode is the plain wave mode, with $m = 0$ and $n = 0$, which propagates at zero spiral angle and with an axial phase speed equal to the speed of sound. Higher radial mode orders are associated with higher mode wavenumbers, higher spiral angles and lower axial wavenumbers. Modes with a critical mode wavenumber equal to k have a 90 degree spiral angle and propagate with wavefronts that are parallel with the walls. Modes with higher than critical mode wavenumbers are cut-off and do not propagate. Only a finite number of modes at any given frequency are cut-on.

circumferential mode order	m
radial mode order	n
mode wavenumber	k_{mn}
rotational phase speed	ω/m
cut-off ratio	$\gamma = k/k_{mn}$
spiral angle	$\sin\phi = 1/\gamma$
axial wavenumber	$k_x = k\cos\phi$

Table 3.1: The important variables of a spinning acoustic mode

Fan/stator interaction contains rotational symmetries that cause only modes of only certain circumferential mode orders to propagate. The mode orders present in the disturbance m are related to the number of fan blades B, the number of stator vanes V and the harmonic of BPF h and are given by the formula

$$m = hB - kV \quad \text{where } k \text{ is any integer} \tag{3.2}$$

3.2 Controller Requirements

A single discrete noise control device, whether passive or active, will react to the acoustic modes of the disturbance and produce, in effect, a scattered sound field. Although, the sound energy of the disturbance may be concentrated in a few of the potential modes of propagation, a single control device can scatter that energy into all of the N possible modes of propagation.

An active noise control system must take into account the full set of N acoustic modes that it could potentially generate. In order to control any or all of the N modes, a modal active control system will require N independent control actuators.

A typical turbofan engine has many hundreds of possible acoustic modes and the hundreds of actuators and independent control channels that would be required for a full modal control system makes its implementation impractical. Fortunately, the number of modes generated by the disturbance N_S is usually much less than N due to the symmetries of fan/stator interaction. A control system that uses a radially symmetric array of actuators can make use of the same mechanism to couple into the same set of modes as the disturbance, without coupling to any of the other modes. Such a system, based on matched symmetrical actuator arrays, results in a much simpler controller.

A circumferential array of L identical actuators, with the same axial and radial coordinates, can be driven by a single control signal, phased appropriately for the position in the array, to produce a set of modes with the same circumferential mode

order m. From the perspective of the controller, the array is a single actuator. However, a problem with such an actuator array is the phenomenon of spatial aliasing. If the array is driven to generate a mode of order m, it will also generate modes of orders

$$\ldots, m - L, m, m + L, m + 2L, \ldots$$

If the mode order of the highest circumferential mode that can propagate is M_N, then at least

$$L > M_N + |m|$$

actuators are required to avoid spatial aliasing.

An important observation is that a single actuator array can independently control multiple m orders when the outputs of two or more phased arrays are summed at each actuator. The number of actuators required is then based on the largest m order.

If, as is usual, the fan blade B and vane V counts are chosen such that at most one m order is cut-on (at least for lower harmonics of BPF), then we can be sure that an array V actuators will not alias as it will produce the identical set of aliased modes as the vanes. There may be circumstances, with disturbances of lower m order, where it may be possible to reduce the number of actuators required in a circumferential array.

Although, the source may only contain modes with one or few m orders, there may be modes of more than one radial order n. In order to couple directly with a given m order, a circumferential array must be placed at the same radial location. To control multiple n orders multiple arrays are required. These must be located at either different axial or radial locations.

Arrays placed at the same radial location but different axial locations, for example both on the duct wall, will couple with a given n order with the same magnitude but different phase. This phase difference is related to the axial phase speed of the mode and is different for different n orders. If the largest number of radial modes of circumferential mode order m is N_m then N_m axial arrays are required.

Arrays placed at the same axial location but different radial location, for example on the inner and outer duct wall or across the radius in the stator vanes, will also couple with a given n order but have the advantage of coupling to both gain and phase as opposed to just phase for wall mounted actuator arrays. Again N_m arrays will be required.

By a similar argument, it is necessary to have two sets of arrays at different axial locations to control modes that propagate in the two axial directions, to the inlet and to the exhaust.

Radial arrays of actuators on the stator vanes have the added advantage of coupling to the modes in the same manner as the disturbance source as they are more or less at the same location. This could potential lead to a requirement for fewer actuators, as a single array could couple fore and aft propagating modes with the same magnitude and phase as the disturbance; a single array could control both modes at the same time. It is conceivable, that a single vane array could couple with multiple disturbance n orders in the same way.

In general, if there are N_S disturbance source modes, then N_S circumferential arrays of actuators are required to independently control each mode.

The effect of using control actuator arrays is that potentially fewer actuators are required than the N theoretically required for full modal control. The main advantage is that the number of controller output channels L is greatly reduced. For exact control we require that $L = N_S$, the number of disturbance source modes. L_A, the total number of individual actuators in the L arrays, can be much larger ($L_A = N_S V$ is usually sufficient) and may in fact be greater than N.

A control system needs to measure the effect of its output in order to be able to adjust that output to achieve noise reduction. This monitoring is implemented by placing residual sensors in the sound field, typically on the duct walls.

Similar arguments to those used to specify the actuator requirements apply to specifying the sensor requirements. In general, in order to sense each of the N modes of propagation, N sensors are required. In order to unambiguously detect modes of a given m order then a circumferential array of

$$M > M_n + |m|$$

sensors are required. If it is known that only N_S independent modes are present, and the mode characteristics are known, then only N_S sensors are required to resolve those modes. In theory, these actuators need not be placed in either circumferential or axial arrays, they can be individual sensors (there are however some restrictions on their locations.)

The use of actuator arrays that allow particular m order components of the disturbance to be resolved would have an advantage if the actuator arrays were imperfect. The ability to separately monitor both the modes of the disturbance and the spillover modes could then assist in preventing spillover. Also, if particular mode components were more important for noise control than others, control could be focused on those modes.

3.3 Control Strategy for the ANCF Rig

The control strategy selected for the ANCF was chosen to meet the requirements of the specific test conditions. The ANCF fan is four feet in diameter and has 16 blades [9]. Nominal speed is 1886 RPM, resulting in a Blade Passage Frequency (BPF) of 500 Hz and a twice BPF (2BPF) tone of 1000 Hz. Twenty eight fan exit guide vanes were selected for the vane actuator tests. The number of stator vanes was selected so that the BPF tone of fan/stator interaction was cut-off. The 2BPF tone was cut-on and contained two radial components that could propagate to the inlet and exhaust.

Table 3.2 gives the cut-off ratios of modes at 1000 Hz in a four foot diameter duct cylindrical with no flow. Counting all $\pm$ m orders and propagation to fore and aft, a total of $N = 72$ modes can propagate. The highest circumferential mode order is $M_N = 9$. When the effects of flow and the larger hub/tip ratio of the exhaust duct are accounted for a similar number is obtained.

For a 16 blade fan and 28 vane stator, the modes generated by fan/stator interaction will be, by equation 3.2

harmonic	m orders				
1	-68	-40	-12	16	44
2	-52	-24	4	32	60
3	-36	-8	20	48	76

The only disturbance modes at BPF of concern are the $m = -12$ modes which are cut-off at 500 Hz. The dominant 2BPF modes are $m = 4$, of which the first two radial modes $(4, 0)$ and $(4, 1)$ are cut-on at 1000 Hz. The next set of 2BPF disturbance modes, $m = -24$, are cut-off. Including modes that propagate both fore and aft, there are a total of $N_S = 4$ independent disturbance modes at 2BPF. The $m = -8$ modes at 3BPF are also cut-on, however disturbance power is concentrated in the 2BPF tones which are the subject of the control effort.

With the maximum m order of propagating modes $M_N = 9$, then in order to control an $m = 4$, mode a circumferential array size of $L > M_N + |m| = 13$ actuators is required. This would suggest that an array of 14 actuators should be sufficient to avoid spillover. However, as the $m = -10$ mode is close to cut-on, for safety an array size of $L > 19$ was chosen. The smallest symmetrical array of vane actuators of this size is $L = 28$. This array size has two other advantages, it has double the effective output of an $L = 14$ array and also allows for extension to control of the 3BPF modes at $m = -8$ if desired.

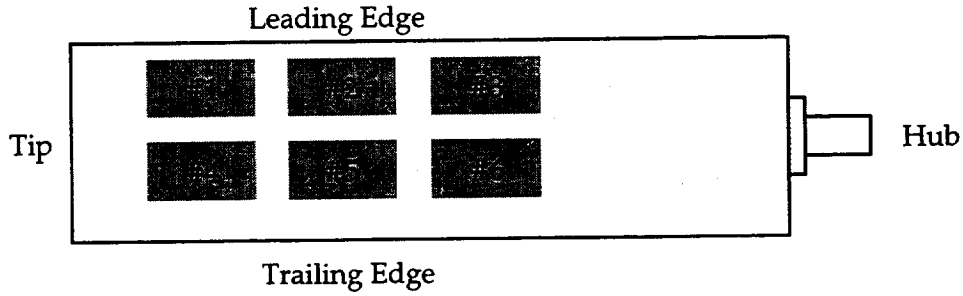

Figure 3.1: Locations of actuators in the vane

As the disturbance has two radial modes then two actuators at two radial locations are required. As it is intended to control sound propagating to both fore and aft, two sets of two actuators at two axial and two radial locations are required.

3.4 Location of Actuators in a Vane

Simulations of the vane actuators required for the ANCF, produced a requirement of a larger inner actuator than outer actuator. Rather than make actuators of two different sizes, it was decided the make the inner actuator from a pair of actuators the same size as the outer actuator. Section 2.9 discusses the selection of actuator size and location. A diagram of the locations of the actuators within each vane is shown in Figure 3.1.

The required four circumferential arrays of actuators were thus constructed from a total of 168 actuators, each of the 28 vanes held 6 actuators each numbered 1 to 6 with actuator #1 being the outer leading edge, #2 the middle leading edge, #3 the inner leading edge, #4 the outer trailing edge, #5 the center trailing edge and #6 the inner trailing edge. The inner pair of actuators on the leading edge, #2 and #3, were driven as a pair with the same control signal making effectively one actuator. In a similar way, the inner pair on the trailing edge, #5 and #6, were also driven as a pair giving effectively four independent actuators on each vane.

Table 3.3 gives the correspondence between the control channels, the labeling of the four outputs of the controller, and the labeling of the location of actuators in each vane (as shown in Figure 3.1)

Power amplifiers were required to drive each of the 168 actuators. As many actuators were driven in pairs by the same control signal, it was decided to pair actuators at the power amplifiers leading to a requirement of 84 amplifiers. The design of the power amplifiers is discussed in Section 2.10.

	n				
	0	1	2	3	4
0	∞	2.91	1.59	1.09	0.84
1	6.05	2.09	1.30	0.95	0.75
2	3.65	1.66	1.12	0.85	0.68
3	2.65	1.39	0.98	0.76	0.63
4	2.09	1.20	0.88	0.70	0.58
m 5	1.74	1.06	0.80	0.64	0.54
6	1.48	0.95	0.73	0.60	0.51
7	1.30	0.86	0.67	0.56	0.48
8	1.15	0.79	0.63	0.52	0.45
9	1.04	0.73	0.59	0.49	0.43
10	0.95	0.68	0.55	0.47	0.41

Table 3.2: Cutoff ratios at 2BPF in a cylindrical duct with no flow. Cut off modes are shaded.

Controller Output Channel	Vane Actuator Location
A1	#1
A2	#4
A3	#2 and #3
A4	#5 and #6

Table 3.3: Correspondence of controller channel and vane actuator location

The two inner actuator pairs on each vane are required to receive the same control signal and so are naturally paired to the output of one amplifier. The outer pair of actuators pose more of a problem as they are individual devices that receive independent control signals. However, when driving an even mode such as an $m = 4$ mode, actuators in the same location of diametrically opposite vanes receive the same control signal (in fact actuators in every seventh vane receive the same control signal) and it was decided to use these to form a pair at the output of one amplifier channel.

3.5 Actuator Phasing

The four circumferential arrays of actuators are driven by four independent controller output signals. In order to drive an $m = 4$ mode, the signal to each of the 28 vanes in an array must be phased appropriately for the location of the vane. The required increment of phase for an $m = 4$ mode is $\frac{2}{7}\pi$. For each array the actuator in the same vane relative to each quadrant, every seventh vane, will receive the same phased control signal; seven independent signals are required for each control channel and its associated array.

The required array phasing was implemented by four sets of seven all-pass digital filters designed to have the correct phase and unity gain at a selected operational frequency, for example 1000 Hz. This phase shifter network was implemented digitally at a fixed sample rate of 6kHz using 24-tap finite impulse response (FIR) filters on a digital signal processing (DSP) computer.

The distribution of the 28 outputs of the actuator array processor to the 84 inputs of the power amplifiers was implemented by hand wiring the filter outputs to the correct amplifier inputs. As the inner arrays have two actuators per vane, each inner array control signal drives eight actuators and four amplifier inputs. Outer array control signals drive four actuators and two amplifier inputs each.

3.6 Vane Wiring Grid

A remaining problem was to connect the 84 amplifier output signals to the correct vane actuator. This was implemented using a large two layer printed circuit board. On one side were 164 signal and 164 signal ground traces for each actuator grouped by vane. On the other side were 164 signal and 164 signal ground grouped by amplifier. The required connections from control amplifier to actuator were made by drilling holes at the correct junction and soldering a contact through the hole.

Table 3.4 is a list of the connections from control channel to actuator.

3.7 Power Amplifier Design

Power amplifiers for PZT actuators such as the THUNDER actuators are a predominantly reactive electrical load, they present the equivalent load of a capacitor to the amplifier. As no commercially available amplifier was available, a custom designed amplifier was built, as described in Section 2.10, with each amplifier channel designed to drive a pair of installed actuators. A total of 88 amplifiers was then required to drive the 168 vane actuators.

An issue with using a single amplifier to drive a pair of actuators is that it becomes difficult to individually calibrate one of the pair if their sensitivities are different as any calibration device must work on the power side of the amplifier at the high voltages used to drive the PZT. A variable resistor is not an option at 100V rms, and so a trim capacitor method was selected.

The amplifiers are current drive devices, that is they produce a given current output for a given voltage input. The two actuators driven by an amplifier were connected in parallel to the amplifier output to ensure that the full voltage output of the amplifier was applied to each actuator.

3.8 Sensor Arrays

A set of sensor arrays constructed by Hersh Acoustical Engineering for this test condition were available and installed on the ANCF rig. There were six circumferential arrays each of sixteen uniformly spaced sensors, three arrays in the inlet labeled A, B and C and three arrays in the exhaust labeled D, E and F. The output of these sensor arrays were processed using an analog beamformer that selected for mode orders $m = \pm 4$.

3.9 Tonal Control

The core control system implements a synchronous multichannel Filtered-X LMS algorithm [7]. The control and plant filters were three tap digital FIR filters.

The plant was identified in the presence of the disturbance in a two step process. The first step designs a set of parallel digital filters that internally cancel the dis-

Amp	Control	Vane	Act	Amp	Control	Vane	Act	Amp	Control	Vane	Act
1-1	A1-1	1	#1	5-1	A3-15	1	#3	9-1	A4-23	2	#5
1-1	A1-1	15	#1	5-1	A3-15	1	#2	9-1	A4-23	2	#6
1-2	A1-1	8	#1	5-2	A3-15	8	#3	9-2	A4-23	9	#5
1-2	A1-1	22	#1	5-2	A3-15	8	#2	9-2	A4-23	9	#6
1-3	A1-2	2	#1	5-3	A3-15	15	#3	9-3	A4-23	16	#5
1-3	A1-2	16	#1	5-3	A3-15	15	#2	9-3	A4-23	16	#6
1-4	A1-2	9	#1	5-4	A3-15	22	#3	9-4	A4-23	23	#5
1-4	A1-2	23	#1	5-4	A3-15	22	#2	9-4	A4-23	23	#6
1-5	A1-3	3	#1	5-5	A3-16	2	#3	9-5	A4-24	3	#5
1-5	A1-3	17	#1	5-5	A3-16	2	#2	9-5	A4-24	3	#6
1-6	A1-3	10	#1	5-6	A3-16	9	#3	9-6	A4-24	10	#5
1-6	A1-3	24	#1	5-6	A3-16	9	#2	9-6	A4-24	10	#6
1-7	A1-4	4	#1	5-7	A3-16	16	#3	9-7	A4-24	17	#5
1-7	A1-4	18	#1	5-7	A3-16	16	#2	9-7	A4-24	17	#6
1-8	A1-4	11	#1	5-8	A3-16	23	#3	9-8	A4-24	24	#5
1-8	A1-4	25	#1	5-8	A3-16	23	#2	9-8	A4-24	24	#6
2-1	A1-5	5	#1	6-1	A3-17	3	#3	10-1	A4-25	4	#5
2-1	A1-5	19	#1	6-1	A3-17	3	#2	10-1	A4-25	4	#6
2-2	A1-5	12	#1	6-2	A3-17	10	#3	10-2	A4-25	11	#5
2-2	A1-5	26	#1	6-2	A3-17	10	#2	10-2	A4-25	11	#6
2-3	A1-6	6	#1	6-3	A3-17	17	#3	10-3	A4-25	18	#5
2-3	A1-6	20	#1	6-3	A3-17	17	#2	10-3	A4-25	18	#6
2-4	A1-6	13	#1	6-4	A3-17	24	#3	10-4	A4-25	25	#5
2-4	A1-6	27	#1	6-4	A3-17	24	#2	10-4	A4-25	25	#6
2-5	A1-7	7	#1	6-5	A3-18	4	#3	10-5	A4-26	5	#5
2-5	A1-7	21	#1	6-5	A3-18	4	#2	10-5	A4-26	5	#6
2-6	A1-7	14	#1	6-6	A3-18	11	#3	10-6	A4-26	12	#5
2-6	A1-7	28	#1	6-6	A3-18	11	#2	10-6	A4-26	12	#6
2-7	-	-	-	6-7	A3-18	18	#3	10-7	A4-26	19	#5
2-7	-	-	-	6-7	A3-18	18	#2	10-7	A4-26	19	#6
2-8	-	-	-	6-8	A3-18	25	#3	10-8	A4-26	26	#5
2-8	-	-	-	6-8	A3-18	25	#2	10-8	A4-26	26	#6
3-1	A2-8	1	#4	7-1	A3-19	5	#3	11-1	A4-27	6	#5
3-1	A2-8	15	#4	7-1	A3-19	5	#2	11-1	A4-27	6	#6
3-2	A2-8	8	#4	7-2	A3-19	12	#3	11-2	A4-27	13	#5
3-2	A2-8	22	#4	7-2	A3-19	12	#2	11-2	A4-27	13	#6
3-3	A2-9	2	#4	7-3	A3-19	19	#3	11-3	A4-27	20	#5
3-3	A2-9	16	#4	7-3	A3-19	19	#2	11-3	A4-27	20	#6
3-4	A2-9	9	#4	7-4	A3-19	26	#3	11-4	A4-27	27	#5
3-4	A2-9	23	#4	7-4	A3-19	26	#2	11-4	A4-27	27	#6
3-5	A2-10	3	#4	7-5	A3-20	6	#3	11-5	A4-28	7	#5
3-5	A2-10	17	#4	7-5	A3-20	6	#2	11-5	A4-28	7	#6
3-6	A2-10	10	#4	7-6	A3-20	13	#3	11-6	A4-28	14	#5
3-6	A2-10	24	#4	7-6	A3-20	13	#2	11-6	A4-28	14	#6
3-7	A2-11	4	#4	7-7	A3-20	20	#3	11-7	A4-28	21	#5
3-7	A2-11	18	#4	7-7	A3-20	20	#2	11-7	A4-28	21	#6
3-8	A2-11	11	#4	7-8	A3-20	27	#3	11-8	A4-28	28	#5
3-8	A2-11	25	#4	7-8	A3-20	27	#2	11-8	A4-28	28	#6
4-1	A2-12	5	#4	8-1	A3-21	7	#3	-	-	-	-
4-1	A2-12	19	#4	8-1	A3-21	7	#2	-	-	-	-
4-2	A2-12	12	#4	8-2	A3-21	14	#3	-	-	-	-
4-2	A2-12	26	#4	8-2	A3-21	14	#2	-	-	-	-
4-3	A2-13	6	#4	8-3	A3-21	21	#3	-		-	-
4-3	A2-13	20	#4	8-3	A3-21	21	#2	-	-	-	-
4-4	A2-13	13	#4	8-4	A3-21	28	#3	-	-	-	-
4-4	A2-13	27	#4	8-4	A3-21	28	#2	-	-	-	-
4-5	A2-14	7	#4	8-5	A4-22	1	#5	-	-	-	-
4-5	A2-14	21	#4	8-5	A4-22	1	#6	-	-	-	-
4-6	A2-14	14	#4	8-6	A4-22	8	#5	-	-	-	-
4-6	A2-14	28	#4	8-6	A4-22	8	#6	-	-	-	-
4-7	-	-	-	8-7	A4-22	15	#5	-	-	-	-
4-7	-	-	-	8-7	A4-22	15	#6	-	-	-	-
4-8	-	-	-	8-8	A4-22	22	#5	-	-	-	-
4-8	-	-	-	8-8	A4-22	22	#6	-	-	-	-

Table 3.4: VaneGrid

turbance tone. These filters are then used to detect the increment in residual microphone signals when each of the four actuator arrays is in turn activated by the controller. The controller then designs a set of 24 filters that model the transfer function from each controller output through each actuator array to each microphone array and controller input. The plant identification can also be run with the fan disturbance noise at a different frequency to the actuator drive signals when a function generator is then used to clock the controller.

The core control is then implemented. This is a synchronous adaptive feedforward scheme based on the Filtered-X LMS. The four output filters were adaptively updated using a function of the output of 24 filters that represent the path from each control output to each sensor input. A feature of the version of the algorithm used for the tests was the ability to set a hard limit to individual control channel output voltages. This was to prevent the control signal from exceeding the maximum level that could safely be accommodated by the power amplifier inputs. The algorithm ensures that the maximum level is not exceeded by preventing any update that would cause a control filter output to exceed that level. The maximum level can be independently set for each control output and if one output is constrained at its maximum, the other control filters can continue to adapt.

The ProANVC monitor program allows interaction with the controller functions to set filter lengths, convergence parameters and control output limits. It also displays in real time the amplitudes of controller output and residual input signals when the control or identification programs are running.

3.10 Control System Schematic

A schematic of all the control system components and their interconnections is shown in figure 3.2.

The control path starts at the sensor arrays, labeled A to F. The 6x16 microphone outputs are processed by the microphone array processor which is implemented in analog electronics. The six outputs of the array processor represent the $m = \pm 4$ component of the sound field at each array location. For each array, two possible outputs were available, the cosine transform component or the sine transform component. When added with the correct phase, these two components can be taken as a time domain representation of the $m = 4$ component. The six processed sensor signals are filtered by analog anti-aliasing filters with a cut-off of 1.1 kHz.

The controller is implemented on a DSP processor. The control algorithm is a synchronous multichannel FX-LMS with off-line identification in the presence of the disturbance. For the test, a 6 input by 4 output control structure is implemented.

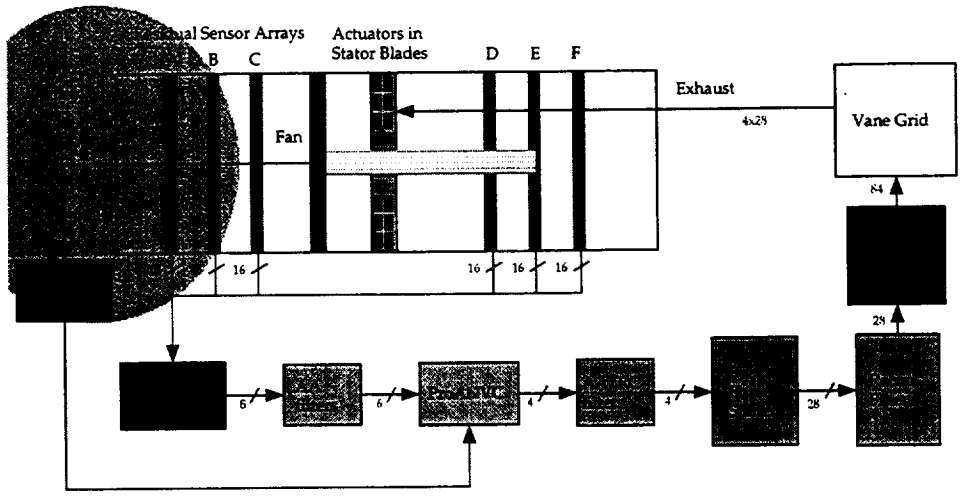

Figure 3.2: A schematic of the control system

The controller is clocked by a signal derived from a digital encoder on the main fan shaft. The encoder produces 128 TTL pulses per fan revolution. As the fan has sixteen blades, this corresponds to a frequency eight times BPF or four times 2BPF, approximately 4 kHz at 1886 rpm. The shaft encoder signal also provided synchronization signals for the rotating rake drive and signal processing system.

The controller is operated in two modes. The first is a synchronous control mode with the fan shaft encoder providing the 4kHz clock for both controller and rake. The second is an asynchronous control mode with an external signal generator providing the clock for both controller and rake. This second mode is used to measure the output of the control system with the fan operating at a different speed. With the fan 2BPF at a different frequency to the actuators, the effect of the actuators alone can be accurately measured by both the controller and the rake system.

For the asynchronous mode of operation, an function generator is used to provide the 4 kHz clock. A schematic of the asynchronous clock processing system is shown in Figure 3.3. The rake controller requires a 4 kHz sine wave which is provided through a signal transformer to the differential input A of the rake controller.

The four controller output signals are passed through four low-pass analog filters with a cut-off of 1.1 kHz. These filters act as reconstruction filters.

The four analog control output signals are then passed to the digital actuator array processor. This is a bank of 28 digital filters designed to have the correct phase shift to generate four independent $m = 4$ mode components at the actuator arrays. The array processor is implements on DSP computer. No anti-aliasing filters are

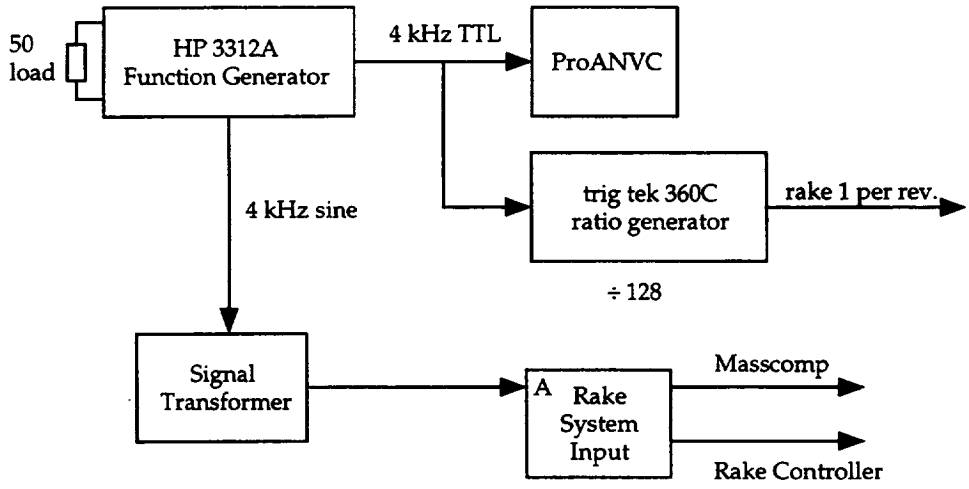

Figure 3.3: Asynchronous clock processing system

required as the control output reconstruction filters suffice. The 28 digital output signals are filtered by a bank of 28 low-pass analog reconstruction filters.

The 28 analog output signals are then taken to and shared by the appropriate inputs of the power amplifiers. The 84 amplifier outputs are then passed to break-out boards attached above each amplifier rack where calibration trimming capacitors can be attached if necessary. The 168 outputs from the break-out boards go the the vane grid where they are distributed to the correct actuators. Twenty eight fifty foot long ribbon cables run from the vane grid to a trailing lead and cable attached to each vane.

Chapter 4

Testing

The test objective was to demonstrate and measure the performance of a ducted fan ANC system based on vane actuators.

4.1 The ANCF Rig

The NASA Active Noise Control Fan facility is located in the Aeroacoustic Propulsion Laboratory at the NASA Lewis Research Center [9].

Figure 4.1 is a diagram of the important components of the ANCF. A sixteen blade four foot diameter fan is enclosed in a fan duct which is cantilevered from a support structure. The fan is driven by a shaft that runs through a center body. As both center body and duct walls are fixed to the support structure, no internal struts are required. (Internal struts could affect the fan/stator interaction acoustic modes of the duct, resulting in a more complicated mode structure.) Inflow and turbulence distortions that would introduce asymmetric force loading of the blades are minimized by an inflow control device at the inlet.

A variable set of stator vanes are cantilevered from a central hub structure. The tips of the vanes are not usually fixed mechanically to the duct wall and due to differences in clearance, some are free and some are jammed against the wall. To avoid variability in their structural dynamics during the tests of vane actuators, the tips of all vanes were fixed to the wall with a strong RTV.

For the tests, the fan blades were set at an angle of 40 degrees. The twenty eight actuator vanes were installed with a 2.25 inch spacing between the fan blades and stator vanes.

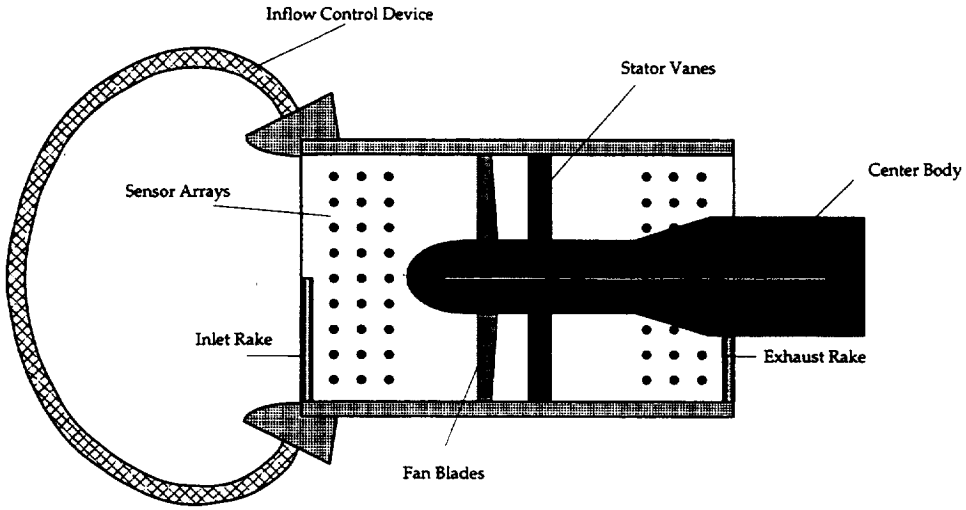

Figure 4.1: Layout of the active noise control fan rig

4.2 Measurements

Two measurements of sound level reduction were made. In duct levels were measured using the NASA rotating rake modal measurement system which allowed the effect of the control system on each propagating mode to be independently measured. Far field measurements were made using a fixed array of 28 microphones.

4.2.1 In Duct Measurements

The propagating modes in a duct are difficult to measure accurately. If N independent spinning modes can contribute to the sound field then an array of at least N independent sensors is required to resolve each and every mode. The rotating rake [8] obviates this requirement by continuously moving a set of fewer microphones while taking data. There are two rake microphone arrays for the ANCF, a seven microphone array for the inlet and a six microphone array for the exhaust. A large gear mechanism installed at each end of the ANCF rig rotates the rakes at one hundredth the rate of the fan (only one rake is installed at a time.) The microphone signals are sampled synchronously with the rotation of the fan and hence synchronously with the interaction spinning acoustic modes generated by the fan.

Time domain averaging is used to reduce noise not synchronized to fan rotation and narrow band spectra are used to extract the magnitude and phase of each m or-

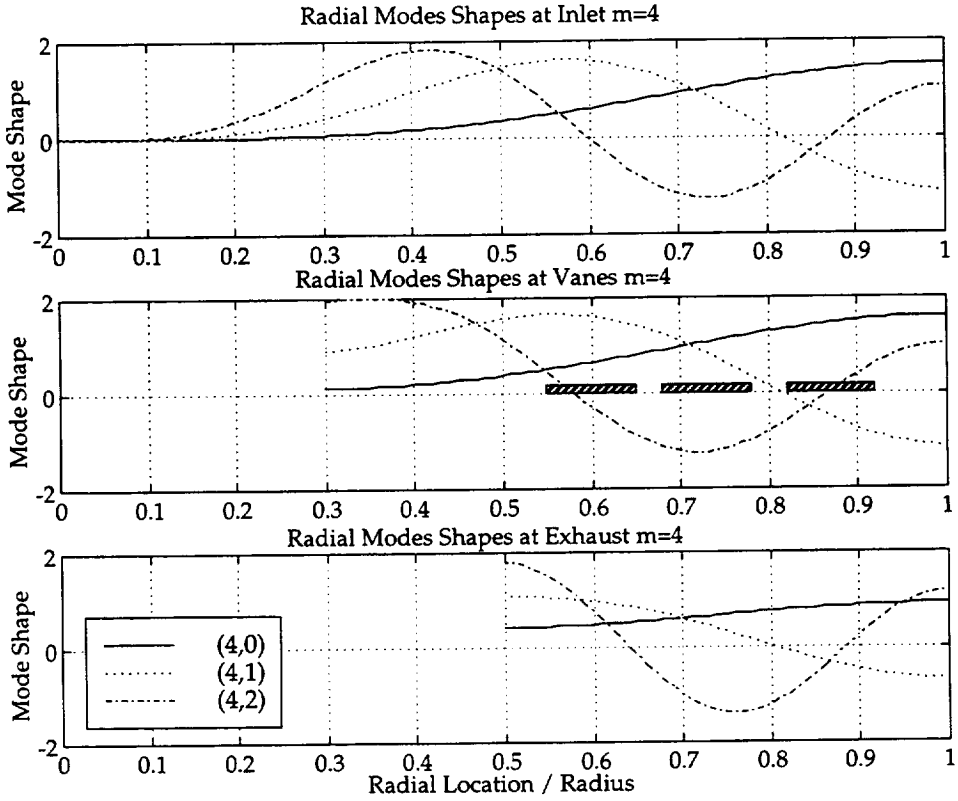

Figure 4.2: Radial mode shapes
The radial mode shapes of the first three components of the $m = 4$ modes at inlet, at the plane of the vanes and at the exhaust. Also shown are patches that represent the radial location of the vane actuators.

der component for each microphone. Different m orders appear as distinct spectral lines frequency shifted due to Doppler effects. A set Bessel functions appropriate to the m order is then fitted to the data in a least squares sense to obtain the radial mode content.

Figure 4.2 illustrates the radial mode shapes for the inlet, vane and exhaust rake locations.

The result of the rake processing is a set of complex spinning mode amplitudes for the sound pressure at the rake locations. It is assumed that reflections from duct terminations are negligible and that the spinning mode amplitudes represent the amplitudes of modes propagating from fan to the duct termination, and then radiating to the far field.

4.2.2 Far Field Measurements

Although the reductions of sound level in the fan duct are of significance, the primary objective of fan noise control is the reduction of the noise radiated to observers in the far field.

The ANCF rig was positioned in the center of the anechoic dome. The radiated sound field is measured at an array of 28 microphones placed in the plane of the fan duct and around a semicircle with a radius of 50 feet.

The far field data cannot distinguish individual spinning mode components. Narrowband spectral analysis was used to detect all tonal components in the sound field at each microphone and BPF, 2BPF and 3BPF components were extracted. The far field data for each BPF tone can be used to determine the directivity of the radiation pattern.

4.3 In Duct Sound Levels

4.3.1 Fan Interaction Modes

The baseline for all in duct sound levels is the sound generated by the fan only, with the control system inactive. This was measured on several occasions and proved to be very repeatable.

Figure 4.3 shows the inlet sound pressure data for measurements taken on four different occasions. Fan speed was 1800 RPM corrected. The result of the least squares fit of the mode shapes to the data is also shown. The sound pressure pattern at the inlet is dominated by the $(4, 1)$ mode; the pattern has a peak at mid span and a node at about 0.84 of the radius that is close to the node of the $(4, 1)$ mode (Figure 4.2). Figure 4.4 shows the fan only exhaust data.

4.3.2 1800 RPM results for the $m = 4$ fan interaction modes

A fan speed of 1800 RPM was chosen as the maximum useful operating speed of the vane actuators. The results of a few experiments at the maximum fan speed of 1886 RPM were disappointing, with power reductions of around 2 dB, possibly due to lack of actuator authority. As results at the slightly lower speed of 1800 RPM were repeatable and acceptable, it was decided to concentrate on tests at 1800 RPM and lower. This section discusses in more detail the results at 1800 RPM and later sections will briefly discuss the lower speed results.

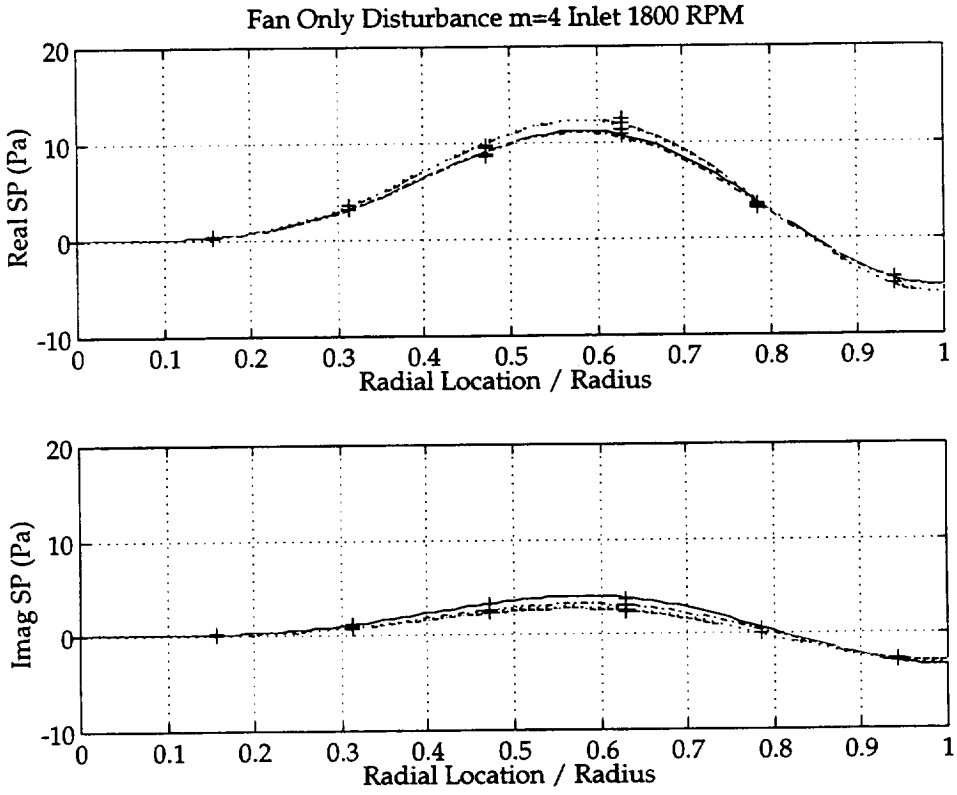

Figure 4.3: Inlet rake fan only sound pressure for 1800 RPM
The fan only sound pressure at the inlet rake for 1800 RPM. Four data set taken on different occasions. The +'s represent measured data. The lines are the result of a least squares fit of the first three radial mode components to the measured data.

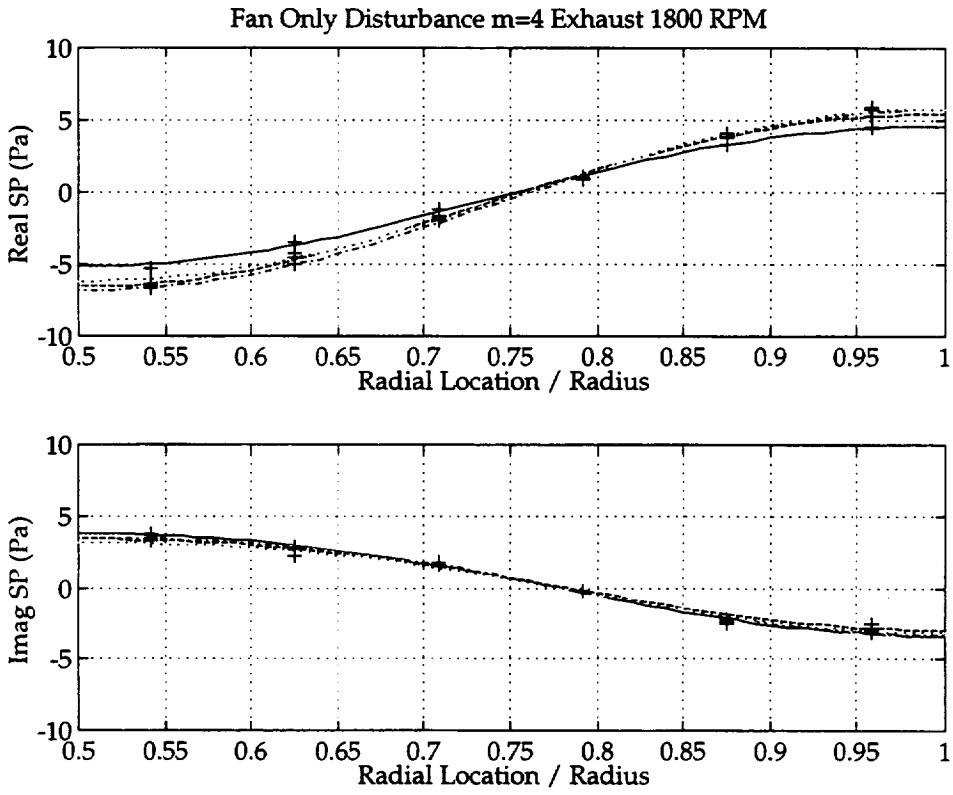

Figure 4.4: Exhaust rake fan only sound pressure for 1800 RPM
The fan only sound pressure at the exhaust rake for 1800 RPM. Four data set taken on different occasions. The +'s represent measured data. The lines are the result of a least squares fit of the first three radial mode components to the measured data.

Run	Sensors	Limit	Mode Power dB		
			(4, 0)	(4, 1)	$m = 4$
2620	Fan Only		96.0	107.8	108.1
2633	ABCDEF	0.5	92.8	100.8	101.5
2622	BCEF	0.75	92.8	98.3	99.4
2632	ABCDEF	0.75	91.8	98.5	99.4
2634	ABCDEF	1.0	92.4	97.8	98.9

Table 4.1: Sound power levels of the $m = 4$interaction modes at the inlet rake for 1800 RPM

Inlet

The controlled sound pressures for several different control parameter configurations is shown in Figure 4.5. The total power in the inlet duct $m = 4$ modes was around 108 dB and control typically reduced the total power to 99 dB, a power reduction in the inlet of 9 dB. The controlled sound power in the modes for this data set is given in table 4.1

The controller used was operated with an output constraint limit that was used to prevent the actuator drive levels exceeding the capability of the power electronics. In a typical experiment, the controller adapted to a solution with one or more output channels at their gain limit, indicating that lack of control authority was limiting the performance of the system (see Section 4.3.3). Several gain limits were used in the experiments with gain limit of 0.5 corresponding to normal operation (actuator drive current of around 85 mA rms) and a gain of 1.0 (170 mA rms) corresponding to the level at which actuator distortion becomes audible.

Run 2620 is the baseline fan only disturbance. Run 2633 is for a controller with the limit set to 0.5 for the maximum output of each control channel. At control convergence, all but actuator array 4 were constrained at their maximum limit indicating that the controller had insufficient authority to completely cancel the fan interaction modes.

When the controller output limit is increased to 0.75 in Runs 2622 and 2632, an extra 2 dB in total power reduction is achieved. Again, all but actuator array 4 were constrained at their new maximum limit indicating that the controller still had insufficient authority. When the controller output limit is increased to 1.0, Run 2634, there is a 0.5 dB improvement in total noise power reduction. Again, all but actuator array 4 were constrained at their maximum limit. A control output limit of 1.0 is considered the maximum feasible gain for the power electronics. At this gain, amplifier distortion is significant and is subjectively apparent as third harmonic distortion of the 2BPF tone (equivalent to a 6BPF tone).

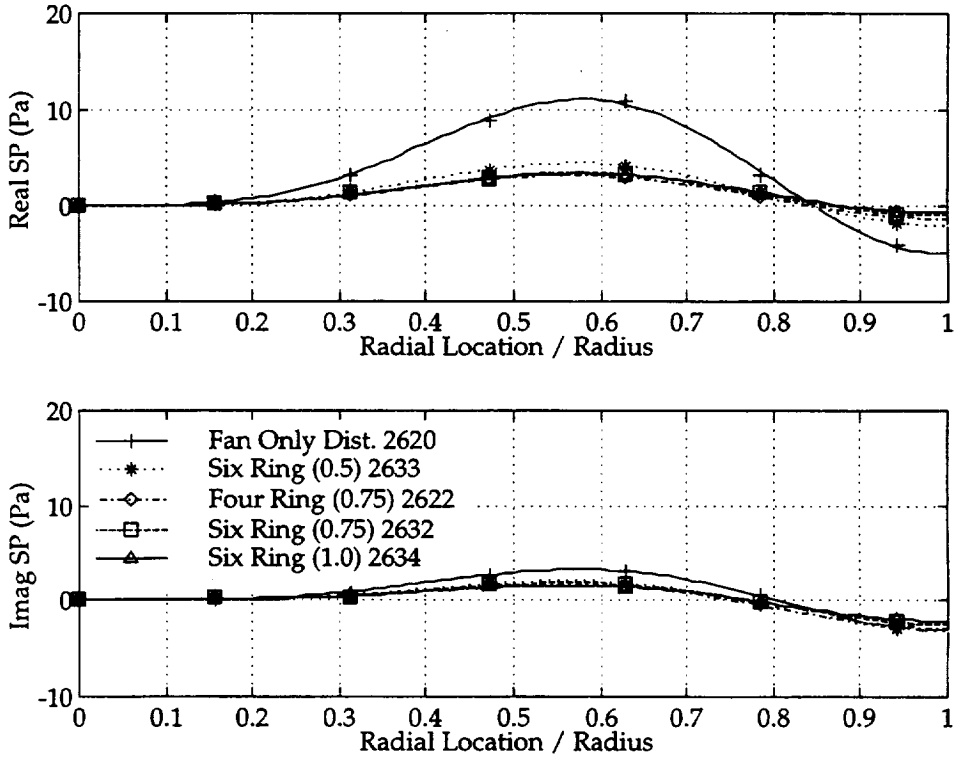

Figure 4.5: Controlled sound pressure, inlet, 1800 RPM
The sound pressure at the inlet rake for 1800 RPM for several different control parameter configurations.

A reduction in mode sound power of 6 dB would indicate that the controller has canceled one half of the disturbance amplitude. As the controller can achieve 6 dB of reduction at a control output limit of 0.5, it is expected that complete cancellation should be possible with a control output limit of 1.0. However, the controller produces a constrained optimization, and a poor condition number of the solution may explain this behavior. Unfortunately, the lack of reliable exhaust transfer function data (see Section 4.3.3) makes evaluation of the true control authority limit infeasible.

The controllers for runs 2622 and 2632 use different sensor arrays. Run 2622 uses four sensor rings, B and C in the inlet and E and F in the exhaust. Run 2632 uses all six rings, three in the inlet and three in the exhaust. As there are only four degrees of freedom in the fan interaction (two modes in the inlet and two in the exhaust), then four sensor rings are sufficient; no improvement in noise reduction is seen when using six as opposed to four sensor arrays.

Exhaust

The controlled sound pressures for several different control parameter configurations is shown in Figure 4.6. The total power in the inlet ducts modes was around 105 dB and control typically reduced the total power to 103 dB, although when control was targeted to the exhaust alone, a controlled power of 99 dB was observed. The controlled sound power in the modes for this data set is given in table 4.2

Run 2707 is the baseline fan only. Run 2708 is for a similar condition to the data for run 2633 described above for the inlet. All six sensor arrays were used. As the inlet levels are higher than the exhaust levels, and the control output is at its maximum limit, the reductions in the exhaust are modest. The controller concentrates its effort on the inlet modes and reduces power in the inlet and exhaust so that they have both approximately the same controlled level. The effect is to reduce the inlet power more than the exhaust power.

When the controller is allowed to target the exhaust modes exclusively, slightly

Run	Sensors	Gain	Mode Power dB		
			$(4,0)$	$(4,1)$	$m=4$
2707	Fan Only		97.7	104.4	105.3
2708	ABCDEF	0.5	94.6	102.1	102.8
2709	DEF	0.5	91.4	97.7	98.6

Table 4.2: Sound power levels for the $m = 4$ interaction modes at the exhaust rake for 1800 RPM

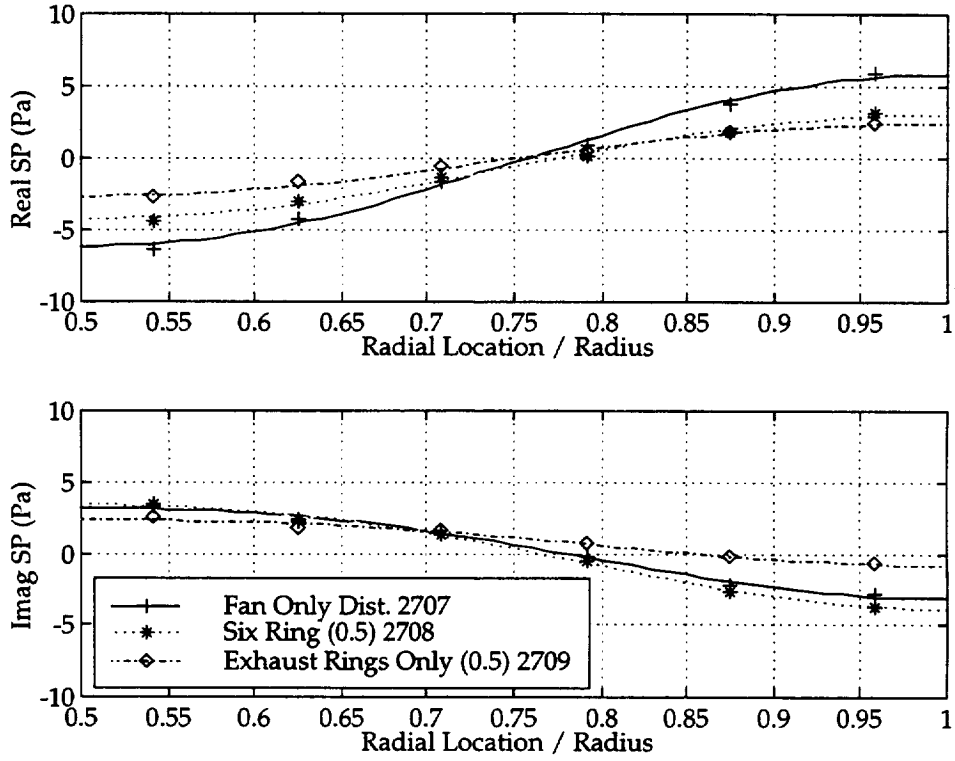

Figure 4.6: Controlled sound pressure, exhaust, 1800 RPM
The sound pressure for the $m = 4$ interaction modes at the inlet rake for 1800 RPM for several different control parameter configurations.

better control is achieved. Run 2709 is the result of controlling just the three exhaust sensor arrays. The control does not 'nail' the modes and is not output limited; the control solution is within the maximum output limit of 0.5.

4.3.3 Control Authority Estimates

A major concern during the project was whether the maximum output of the vane actuators was sufficient to control the fan interaction modes. Predictions, based on simulations 2.9 suggested that the actuators would have just enough displacement to control the fan at full speed. However, although 9 dB total power reductions are possible, the initial data for 1800 RPM and other fan speeds suggests that either there is insufficient control authority to 'nail' the modes or that control modal spillover is generating an artificial noise floor.

In order to determine the level of actuator output that would be required to completely cancel the fan interaction modes, experimental data was taken of the response of the modes to individual actuator arrays; that is the controller transfer functions from actuator array inputs to complex mode amplitudes, with each of the four controller channels activated in turn.

There were two issues in the measurement of these transfer functions. In order to get a good signal to noise ratio, it would be preferable to measure the acoustic modes of the actuator with no fan noise, that is with the fan not running. However, it was discovered that the fan has a large impact on the sound field generated by vane actuators. The fan blade are only 2.25 inches from the stator vanes. When a fan blade is close to a given stator vane, the sound from the actuators in that vane is reflected from the surface of the blade. The total effect is a sound field that is very sensitive to the rotational position of the fan. It was found that by running the fan at idle, a repeatable modal transfer function could be measured, and it is assumed that the effect of the fan location is then randomized and averaged.

The mean flow of air through the duct also has an effect on acoustic mode propagation with upstream modes being shifted to higher wavenumbers and downstream modes being shifted to lower wavenumbers. To include the effect of mean flow on the measurements, the fan was run at approximately 90 percent of the nominal speed and the actuators were driven by a tone equivalent to 2BPF at full speed.

The second concern was that if fan location has such an impact on the acoustic modes produced by the vane actuators, that when the actuators are synchronized to the fan rotation the resulting sound field would not simply be the superposition of the fan interaction sound field and sound field due to the actuators with the fan at idle. The synchronization of fan and actuators would put a fan blade at the same

phase location with respect to the cycling of the signal of a vane actuator, locking the fan phase in a given location. A phase-locked fan could exhibit the same characteristics of a stationary fan, that is the sound field produced could be dependent of the initial phase between actuator and fan. There were some initial indications that a non-linear effect was indeed present; data for actuators only when summed to data for fan only did not equal the data for synchronized actuators and fan.

A set of experiments designed to demonstrate this phenomenon were performed. The actuators were run at a fixed amplitude synchronously with the fan 2BPF. The phase of the actuator signals were then switched though four quadrants and the mode data were taken for each condition. Figure 4.7 plots the resulting inlet and exhaust data. The data for the four quadrants of phase form an approximate square centered on the point that represents the fan only sound field. This demonstrates that there is no significant phasing effect on the amplitude of the modes generated by the actuators.

Having determined that there is no significant fan phasing effect, the actuators arrays (controller channels) were run individually. The control signal was equivalent to the 2BPF tone at 1800 RPM but the fan was run at idle or at 90% of nominal speed.

Figure 4.8 shows the sound pressures at the inlet rake for each actuator array. The two tip actuators arrays A1 and A2 couple mostly into the $(4,0)$ mode and the two hub actuator arrays A3 and A4 couple mostly into the $(4,1)$ mode. The amplitude of the response due to the hub actuators is larger as these are the arrays with two actuators per vane.

The transfer functions are collected into a matrix $\mathbf{C}_i$

$$\mathbf{C}_i = \begin{bmatrix} c_{i,(4,0),1} & c_{i,(4,0),2} & c_{i,(4,0),3} & c_{i,(4,0),4} \\ c_{i,(4,1),1} & c_{i,(4,1),2} & c_{i,(4,1),3} & c_{i,(4,1),} \end{bmatrix}$$

where $c_{i,(4,0),1}$ is the measured complex mode amplitude of the inlet $(4,0)$ mode generated by actuator array A1 and so on.

The fan only interaction modes are collected in the vector $\mathbf{d}_i$ where

$$\mathbf{d}_i = \begin{bmatrix} d_{i,(4,0)} \\ d_{i,(4,1)} \end{bmatrix}$$

If the controlled mode amplitudes in the inlet are $\mathbf{r}_i$ then

$$\mathbf{r}_i = \mathbf{C}_i\mathbf{x} + \mathbf{d}_i$$

where $\mathbf{x}$ is the vector of complex amplitudes of the control signals. This transfer function formulation should enable the prediction of controlled mode amplitudes

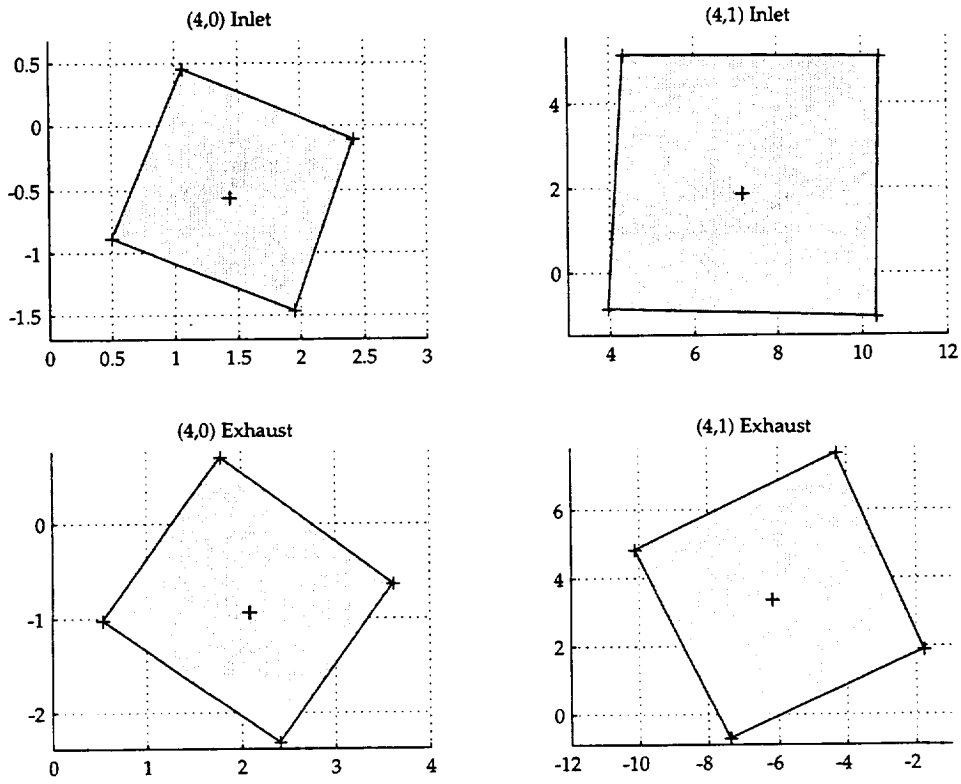

Figure 4.7: Mode amplitudes for a fixed control signal swung though four quadrants of phase.

The complex mode amplitudes for a fixed control signal set swung though four quadrants of phase. The four points form a square centered on the fan only noise. Fan speed 1800 RPM. Control set 1+2-3-4; limit 0.5. Inlet runs 2697 to 2700. Exhaust runs 2668 to 2671.

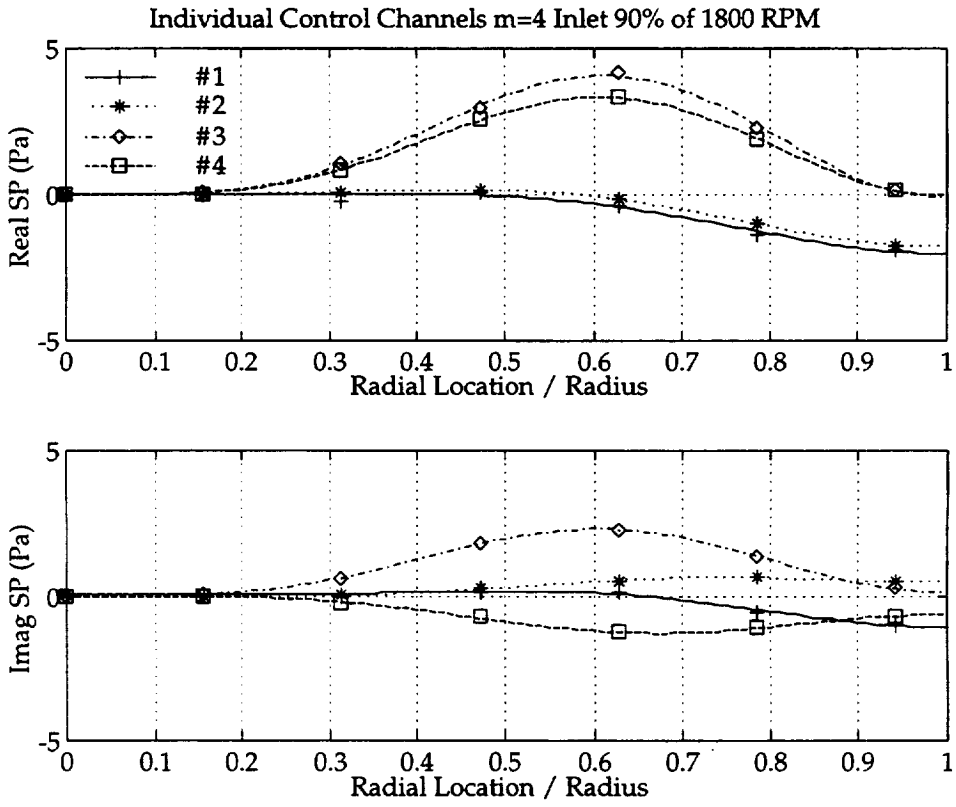

Figure 4.8: Modal response to individual actuator arrays for the inlet
Modal response to individual actuator arrays for the inlet. Excitation at the equivalent of 2BPF at 1800 RPM and the fan at 90 % of that speed.

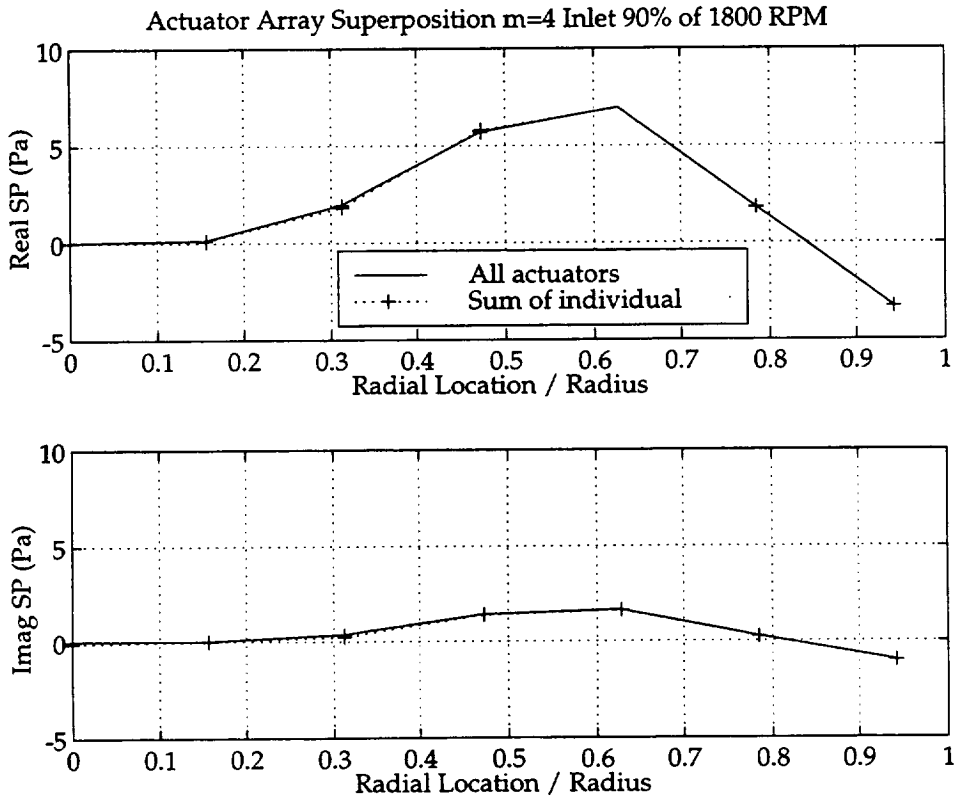

Figure 4.9: Inlet superposition validation
Validation of the principle of superposition for the measured individual actuator array mode transfer functions in the inlet.

for any set of control signals x. A suitable test of this is to compare the measured result of running all actuators at the same time with the sum of the individual measurements for each array. Figure 4.9 shows that this superposition assumption is valid.

The control signal vector that exactly cancels the fan interaction vector can now be found by inverting the transfer function matrix C. As C has two rows (corresponding to the two radial modes in the inlet) but four columns (corresponding to the four actuator arrays, it has many inverses. Of all the inverses of C, we would like to find the one that results in the smallest control vector x. One solution is to use the pseudo inverse of C [10] denoted by C^+ when the required control vector is

$$\mathbf{x_i} = \mathbf{C^+ d_i}$$

When this is done for the inlet data at 1800 RPM, the maximum absolute value of the control vector is 0.99. This would indicate that a control output limit of 1.0 should be sufficient to 'nail' the modes in the inlet.

Unfortunately, a similar set of calculations for the exhaust duct, is not possible. One data set was taken at 90% speed, but it failed the superposition quality check. There were indications in the data of intermittent phase shifts between the controller signal and the rake data processing. This occurred only when the rake data processing received a clock signal driven from the test equipment, as shown in 3.3, as opposed to the normal method of clocking the rake from the fan shaft encoder. This was believed to have been solved by using an isolating signal transformer between the rake processing input and the controller.

As the rake processing uses a clock signal that is four times the period of the control clock signal, shifts of 90 degrees were sometimes observed as a clock pulse was missed by either the controller or the rake data processing. However, a possible phase shift of 45 degrees was observed in this exhaust data set, Figure 4.10, for which no explanation could be formed.

The relative phase of the inlet and exhaust modes is a key determiner of the required control authority. As the phase of the exhaust mode transfer functions is thrown into doubt by the failure of the superposition test, it was also not possible to predict the control authority required to simultaneously control inlet and exhaust modes.

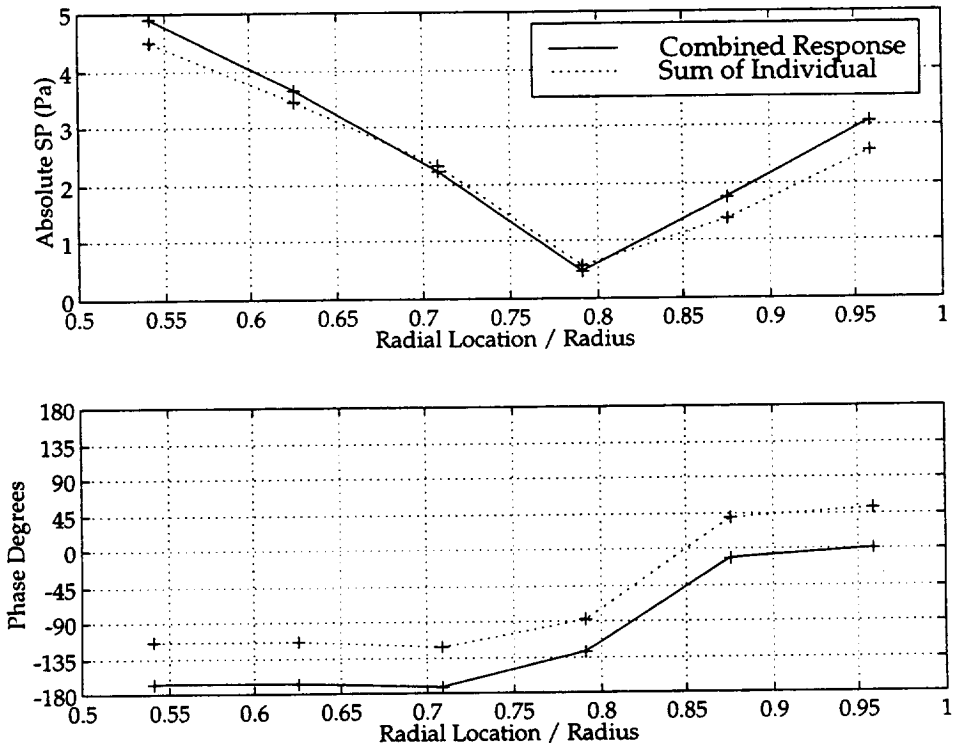

Figure 4.10: Exhaust superposition validation
Validation of the principle of superposition for the measured individual actuator array mode transfer functions in the exhaust. Note the 45 degree difference between the predicted and measured response.

		Inlet			Exhaust		
RPM		(4,0)	(4,1)	m=4	(4,0)	(4,1)	m=4
1800	Fan Disturb	96.0	107.8	108.1	96.6	104.5	105.1
	controlled	91.8	98.5	99.4	92.3	100.9	101.5
1700	Fan Disturb	97.1	106.5	107.0	93.2	105.1	105.4
	controlled	92.3	100.9	101.5	94.6	101.6	102.4
1600	Fan Disturb	90.7	107.5	107.6	89.3	104.1	104.3
	controlled	87.9	101.3	101.5	90.3	99.4	99.9
1500	Fan Disturb	90.8		90.8	95.2	90.9	96.5
	controlled	73.0		73.0	90.1	81.3	90.7
1400	Fan Disturb	103.4		103.4	96.8		96.8
	controlled	83.9		83.9	86.9		86.9

Table 4.3: Acoustic mode powers for the fan interaction and the controlled sound fields for lower RPM. (Gain limit 0.75)

4.3.4 Lower Fan Speeds

The results of applying control at lower fans speeds were similar to those for 1800 RPM. Four additional fan speeds were investigated 1700, 1600, 1500 and 1400 RPM. The data are summarized in Tables 4.3. When the speed falls to 1500 RPM, only one fan interaction mode can propagate in the inlet and at 1400 RPM only one mode in can propagate in the exhaust. At these speeds the four actuator arrays have more than enough authority to cancel the inlet mode. Of note, however, is the inability of the system to produce large reductions in the exhaust.

The data from Table 4.3 is also shown in Figures 4.11 and 4.12. The darker bars in these figures represent the fan only disturbance levels of the $(4, 0)$ and $(4, 1)$ modes and their combined power. Superimposed are lighter bars that show the residual levels.

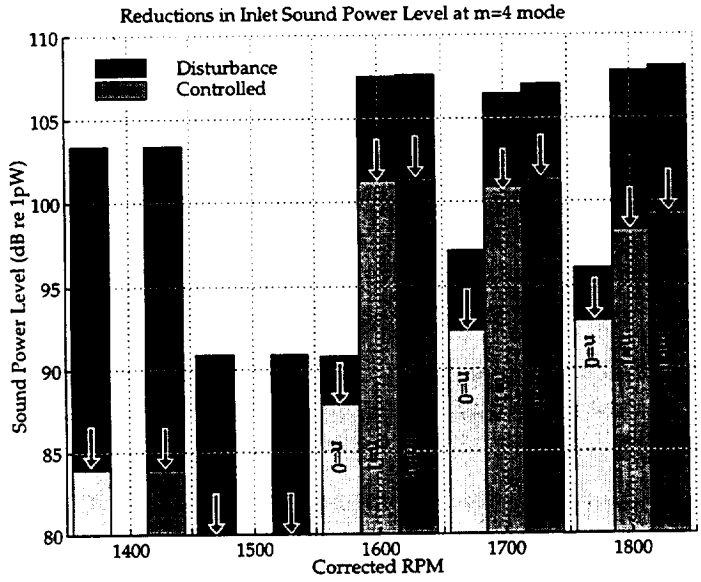

Figure 4.11: Fan only disturbance and controlled residual levels of the $m = 4$ modes at the inlet for a range of fan speeds.

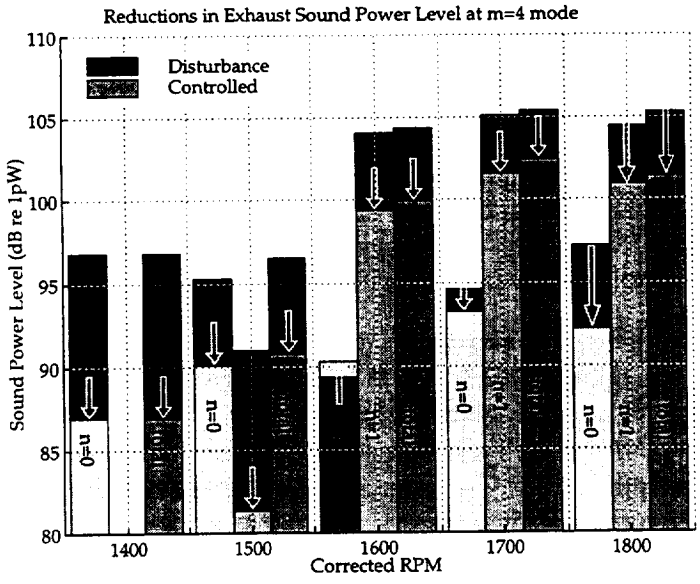

Figure 4.12: Fan only disturbance and controlled residual levels of the $m = 4$ modes at the exhaust for a range of fan speeds.

4.4 Spillover

4.4.1 The Causes of Spillover

The vane actuator ANC system relies on the mechanism of source mode matching. The system aims to generate the same modes as the fan/stator interaction disturbance and to generate *only* those modes, and it does this by phasing the control signals to the actuators in order to spin the specific modes required. The residual sound caused by errors in the matching of the modes is called spillover.

Spillover is a common feature of modal control systems and comes in two flavors, observer spillover caused by limitations in sensing and control spillover caused by limitations in actuation.

The most important source of spillover in the vane actuator ANC system is *control spillover* in the form of contamination of the mode generation of the source array by errors in the array processing. The most common source of these errors is differences in the sensitivity (in both magnitude and phase) of the actuator elements that make up each array.

In a perfect system, the differences in the sensitivity of elements would be compensated by calibration of the array processing system. Each element of an array requires a separate adjustment of both the gain and phase of its input signal.

For the vane actuator ANC system, the ideal location to introduce calibration of the 168 actuators, was in the unique signal path to an individual actuator. Unfortunately, as two actuators shared a common power amplifier, the only unique signal path was the high voltage lead at the amplifier output. A high voltage potentiometer would be bulky and would draw a lot of electrical power and so was deemed impractical for our application and an alternative method using trimming capacitors was developed.

The vane actuators present a capacitive load to the amplifiers which are current sources. A high voltage trim capacitor placed in parallel with an actuator can be used to shunt some of the current and equalize the sensitivity of an array of actuators to the sensitivity of the weakest element. As the amplifiers have a power limit, reducing the sensitivity of array elements also reduces their maximum response. During the experiments, maximizing the response of the actuators had a higher priority than minimizing spillover and the trimming capacitors were not used.

Additional calibration was possible at the input to each power amplifier, Figure 3.2. At this point in the control loop there were 84 low voltage signals, each of which supplied a power amplifier for two individual actuators. For vane actuators #1

		Sound Power Level (dB)				
Actuator	Gain	m=4	m≠4	Total	Spillover	Run No
#1	0.5	95.6	88.7	96.4	−6.9	2680
#2	0.5	93.9	88.4	95.0	−5.5	2681
#3	0.5	101.2	83.4	101.2	−17.8	2682
#4	0.5	99.2	90.0	99.7	−9.2	2683
all	0.25	98.5	92.6	99.5	−5.9	2684
all	0.5	104.1	98.1	105.1	−6.0	2685
all	0.75	106.6	100.8	107.6	−5.8	2686
all	1.0	107.3	101.6	108.4	−5.7	2687

Table 4.4: Spillover in the inlet at 1 kHz

and #4, one amplifier powered actuators on vanes diametrically opposite to each other. For vane actuator pairs #2 and #3, and #5 and #6, each amplifier powered the appropriate pair on individual vanes. A potentiometer at the input to each power amplifier was trimmed to approximately equalize the output of the actuators in each array, with the limitation that pairs of actuators could not be individually calibrated, only trimmed as a pair.

A further layer of possible calibration was at the array processing (digital phase shifter), where the gain and phase of the 28 array output signals could be adjusted. This calibration layer was not used during the experiments.

In order to assess the degree of control spillover from the actuator arrays, each array was activated in turn with the fan running at 90% of full speed. The rotating rake data acquisition system was synchronized to the 1 kHz signal driving the actuators. In this way, the rake processing averaged out unsynchronized fan tones leaving just the sound due to the actuators.

Table 4.4 shows the spillover for each actuator array in the inlet. Three sound power measurements are shown, the power in the target m=4 modes, the power in all other circumferential modes and the total power in the 1 kHz tone. The spillover column is the ratio of the power in the unwanted modes to the power in the target mode.

The spillover for each actuator array varies as each array has a slightly different calibration. Array #3 is the best with a spillover of -17.8 dB. Array #2 is the worst with a spillover of -5.5 dB. The mode mix for of these two cases is shown in Figures 4.13 and 4.14.

Table 4.4 also shows the spillover for the set of all actuators run together which gives a measure of the average over the set and the spillover that might be expected when all four arrays are used to control a disturbance mode. (The exact

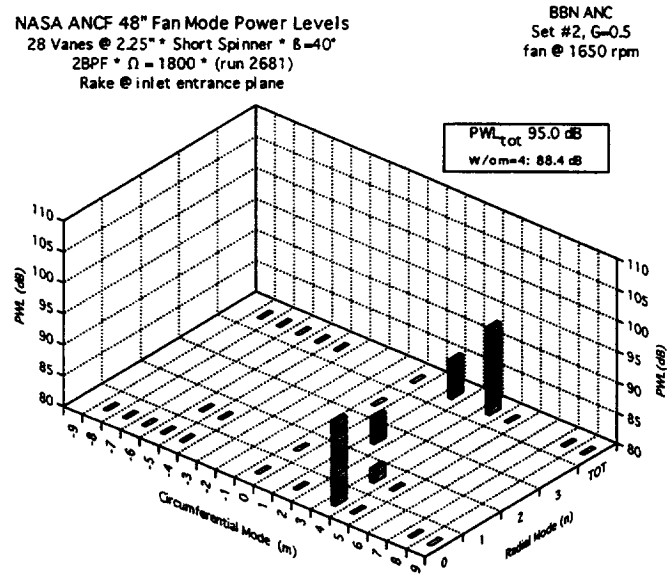

Figure 4.13: Mode mix for actuator array #2 at 1 kHz in the inlet.

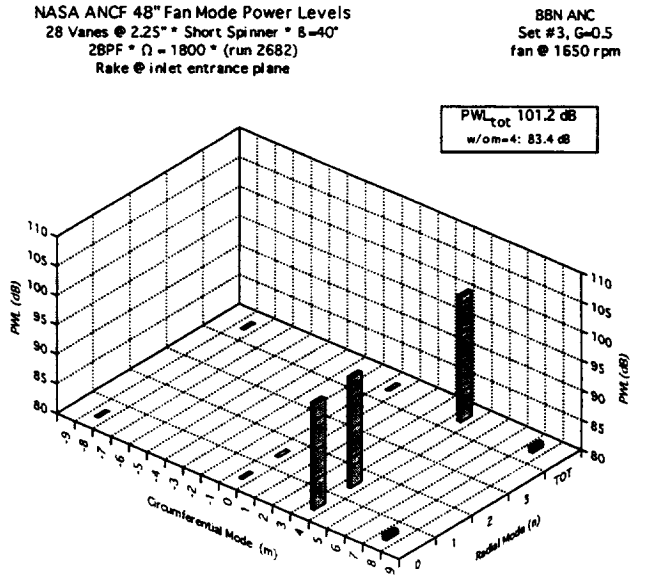

Figure 4.14: Mode mix for actuator array #3 at 1 kHz in the inlet.

		Sound Power Level (dB)				
Actuator	Gain	m=4	m≠4	Total	Spillover	Run No
#1	0.5	85.8	85.1	88.5	−0.7	2688
#2	0.5	92.7	84.4	93.3	−8.3	2689
#3	0.5	94.9	86.0	95.4	−8.9	2690
#4	0.5	96.4	83.5	96.7	−12.9	2691
all	0.25	95.0	91.8	96.7	−3.2	2692
all	0.5	100.5	97.7	102.3	−2.8	2693
all	0.75	102.9	99.6	104.6	−3.3	2694

Table 4.5: Spillover in the exhaust at 1 kHz

spillover during control will depend on the control solution and the exact mix of actuator arrays used. The mix used here was chosen to be close to observed control solutions.) The level of drive signal to the actuators was varied to determine how the level of spillover changed with drive level, with a gain of 0.5 corresponding to normal operation (85 mA rms) and a gain of 1.0 (170 mA rms) corresponding to the level at which actuator distortion becomes audible. The average spillover is -6 dB and surprisingly does not increase when the actuators are over driven.

Table 4.5 shows the spillover for each actuator in the exhaust. As we have the same experimental conditions as for the inlet spillover data, the actuators are being driven by the same signal into the same flow condition, we might expect that the spillover in inlet and exhaust be the same. However, this is not the case.

The acoustic modes in the inlet and exhaust are driven by the same source mechanism under the same condition. In the plane of the vanes, the source mechanism must have the same spillover characteristics in each case and so the differences between inlet and exhaust must be in the propagation from the source to the rake planes. In addition, the propagation path must be different for different modes to account for the difference in ratios of m=4 modes to other modes in the spillover measure. Causes of the difference in propagation might include differences in mode impedance due to the different duct cross-sections, difference in reflection (and radiation) properties at the exit planes and also difference in coupling due to the orientation of the source dipoles.

That the vanes generate different sound levels in inlet and exhaust can be seen in the levels of the target m=4 mode power levels which are typically 3 dB higher in the inlet. This also is the typical difference in level for the fan only disturbance in these modes which is perhaps not surprising as both vane actuators and blade/stator interaction generate sound from the same source region.

In table 4.5, actuator array #1 has by far the worst spillover at =-0.7 dB. The mode

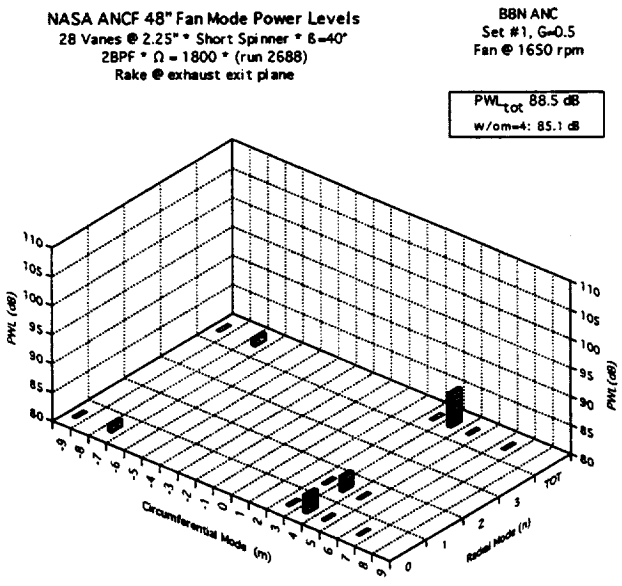

Figure 4.15: Mode mix for actuator array #1 at 1 kHz in the exhaust.

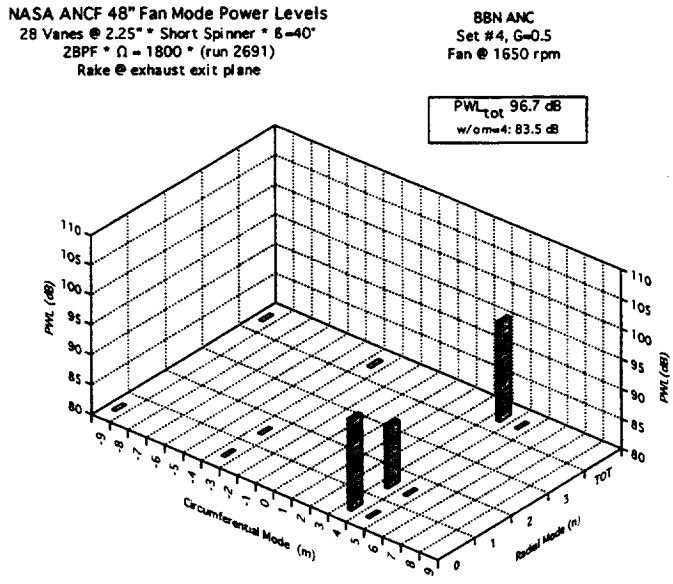

Figure 4.16: Mode mix for actuator array #4 at 1 kHz in the exhaust.

mix for this array, together with that for array #4 is shown in Figures 4.15 and 4.16. The poor spillover performance of #1 is almost certainly due to the m=4 level which is the lowest of any array and is close to the noise floor which is 85 dB for this data set. The other three arrays have less than -8 dB spillover which is comparable to the spillover of individual arrays in the exhaust.

Also shown in Table 4.5 are the spillover levels for all the actuators run together at different gain levels. As before the spillover is the same for low and high drive levels, but at an average of -3 dB is far higher than might be expected from the contributions of the individual arrays. In fact, the spillover power for all actuators run together at 97.7 dB is higher that the coherent sum of the spillover power for each actuator which is 96.8 dB. We might expect the modal response of non-target modes to each actuator array to be random in magnitude and phase and hence for the spillover powers to add incoherently (the incoherent power sum is 90.9 dB). This is a puzzle.

A possible explanation is error in the method of calculating spillover power for different absolute power ranges. The response to individual actuators is lower and more mode levels are below the noise threshold and so are not counted in the spillover total. The combined response brings those discounted modes above the noise threshold and so they are then counted, leading to a large jump in calculated spillover.

4.4.2 The Effects of Spillover

Control spillover degrades the performance of the noise control system. How much it degrades the performance depends on the performance measure (target mode, total sound power (in-duct) or radiated sound power) and also on how the control system determines its solution.

The control system gathers its knowledge about its own performance from its sensor arrays. Limitations in the ability of the sensor arrays to measure the modal content of the sound field are the manifestation of the second flavor of spillover, observer spillover. Observer spillover typical occurs due to calibration errors in sensor arrays (but can also occur due to spatial aliasing, which is also a potential source of control spillover).

The accuracy of the rotating rake measurement system used to present performance results for the in-duct sound field, means that observer spillover is not an issue for the presentation of in-duct results. However, observer spillover could be an issue with the sensor arrays used by the control system. These arrays were designed to filter the $m = 4$ modes (in practice only 8 sensors were used in each array

and so the filter was sensitive to both $m = 4$ and $m = -4$ modes), and calibration errors would lead to other modes being superimposed on the measurement.

An ideal sensor array, perfectly tuned to the target mode, would cause the control system to optimize its performance to reduction of the target mode, even in the presence of control spillover. The resulting control solution may produce very good reductions of the target modes, but have poor reductions in the total sound power due to the generation of the spillover modes by the actuators.

A sensor array subject to observer spillover will prevent the control system from achieving a true minimum in the sound power of the target modes. However, if the spillover makes the array more sensitive to total power in the tone, the reductions in total power may be greater with spillover than with a perfectly tuned sensor array. In the limit of a sensor that is a total power sensor, the control system will optimize its performance to the reduction of total power, even in the presence of control spillover. Of course, the reduction achieved will be determined, and be limited by, the control spillover.

A little analysis can clarify these conclusions. Assume that the fan/stator interaction generates a single target mode of amplitude m_0 and a single spillover mode of amplitude n_0. The total power of the disturbance P_0 will be

$$P_0 = m_0^2 + n_0^2$$

Assume that the actuator arrays generate a target mode amplitude of m_1 and a single spillover mode of amplitude n_1 and that there is a single control gain α such that the residual target mode amplitude is $m_0 - \alpha m_1$. The residual power P_1 will then be (assuming that the two spillover modes are not coherent)

$$P_1 = (m_0 - \alpha m_1)^2 + \alpha^2 n_1^2 + n_0^2$$

The target mode is eliminated if

$$m_0 - \alpha m_1 = 0$$

However, this results in a residual total power

$$P_1 = \frac{n_1^2}{m_1^2} m_0^2 + n_0^2 = \sigma m_0^2 + n_0^2$$

where σ is the spillover measure $\frac{n_1^2}{m_1^2}$. The residual total power is minimize if

$$\alpha(m_1^2 + n_1^2) - m_0 m_1 = 0$$

resulting in the smaller residual total power

$$P_1 = \frac{\sigma^2}{(1+\sigma)^2} m_0^2 + \frac{\sigma}{(1+\sigma)^2} m_0^2 + n_0^2 = \frac{\sigma}{1+\sigma} m_0^2 + n_0^2$$

Note that at the condition of minimum total power, the power in the control spillover is *greater* than the power in the target tone by a factor of σ. Given a σ of -6 dB for the inlet and -3 dB for the exhaust we would expect reductions in total power to be -6 dB in the inlet and -3 dB in the exhaust if the sensor arrays were perfectly tuned to the target mode. For total power sensors we would expect reductions in total power of -7.0 dB in the inlet and -4.8 dB in the exhaust.

Tables 4.6 and 4.7, and Figures 4.17 and 4.18, give measured disturbance and residual sound power levels in the inlet and exhaust for the target $m = 4$ mode, the spillover modes and the total 2BPF tone for a range of fan speeds. As expected, in all cases, the spillover power increases in the controlled sound field and the residual $m = 4$ level is less than the residual tone level. For example, figure 4.20 shows the measured modes at the inlet plane for 1800 RPM with the control system on. Contributions from spillover modes can be seen at $m = 2, 5, 7$ and $m = 8$. That these must have been generated by the actuators can be seen by comparison with the control off condition shown in 4.19 which shows the dominant $m = 4$ modes due to fan/stator interaction with little or no spillover. Data from other speeds and conditions is similar.

In the inlet, the residual tone power at 1800 RPM level, at -6.4 dB, is consistent with the measured spillover. However, the target tone power is still greater than the spillover power and so control spillover is not limiting performance. In the exhaust, the residual tone power is greater than would be expected from the spillover measurement.

Something other than control spillover is limiting performance in the inlet and exhaust. As discussed before, the limit in the exhaust may be simply the power balance between inlet and exhaust, exhaust performance is limited because inlet performance is limited. The limitations in the inlet may be due to actuator power limitations or perhaps misadjustment in the control solution due to either insufficient convergence time, random control perturbations or control sensor errors.

At lower fan speeds, at 1400 and 1500 RPM, the tonal power is significantly reduced and its residual level is comparable to the level of the spillover modes. This suggests that control spillover is slight at these speeds but that spillover is the limiting factor on performance. The spillover may be smaller simply because fewer modes are cut-on at the 2BPF frequency.

	m=4			Tone			m≠4		
RPM	Off	On	±	Off	On	±	Off	On	±
1400	103.4	83.9	−19.6	103.5	89.4	−14.1	84.0	88.0	+4.0
1500	90.8	73.0	−17.8	91.9	89.3	−2.6	85.5	89.3	+3.8
1600	107.6	101.5	−6.1	107.7	101.8	−5.9	91.0	90.9	−0.1
1700	107.0	101.5	−5.5	107.1	102.8	−4.3	91.6	93.9	+2.3
1800	108.1	99.4	−8.7	108.2	101.8	−6.4	93.1	98.1	+5.0

Table 4.6: Controlled Power Levels of m=4 tone, spillover and 2BPF tone in the inlet for a range of fan speeds.

	m=4			Tone			m≠4		
RPM	Off	On	±	Off	On	±	Off	On	±
1400	96.8	86.9	−9.9	97.1	86.9	−10.2	85.8	86.9	+1.1
1500	96.5	90.7	−5.9	96.8	94.8	−2.0	84.8	92.7	+7.9
1600	104.3	99.9	−4.4	104.3	100.7	−3.6	86.1	93.2	+7.1
1700	105.4	102.4	−2.9	105.5	103.5	−2.0	91.7	96.9	+5.2
1800	105.3	102.9	−2.4	105.4	103.4	−2.0	89.5	93.8	+4.3

Table 4.7: Controlled Power Levels of m=4 tone, spillover and 2BPF tone in the exhaust for a range of fan speeds.

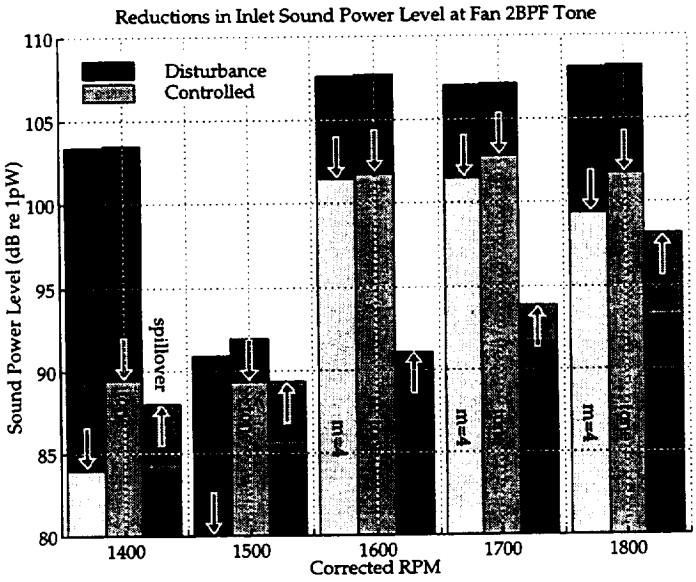

Figure 4.17: Spillover in the inlet.

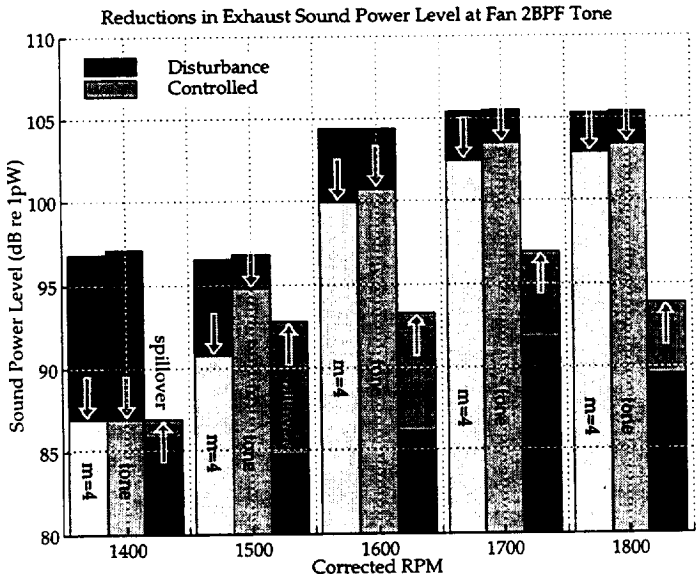

Figure 4.18: Spillover in the exhaust.

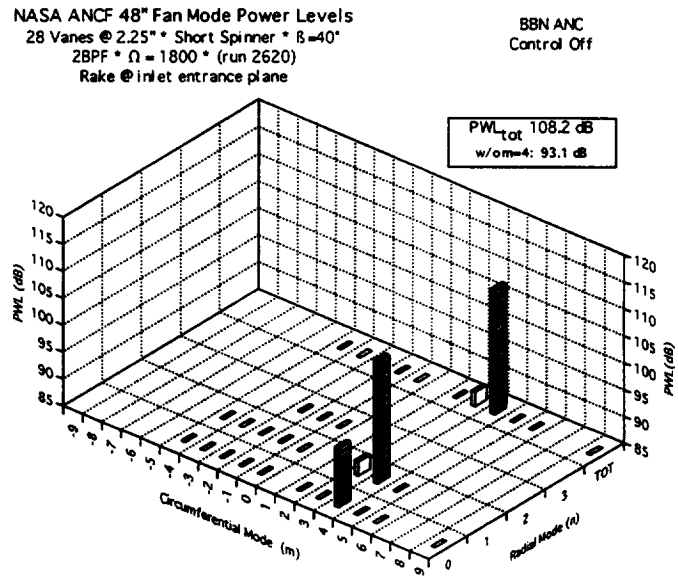

Figure 4.19: Fan only mode mix at 1800 RPM

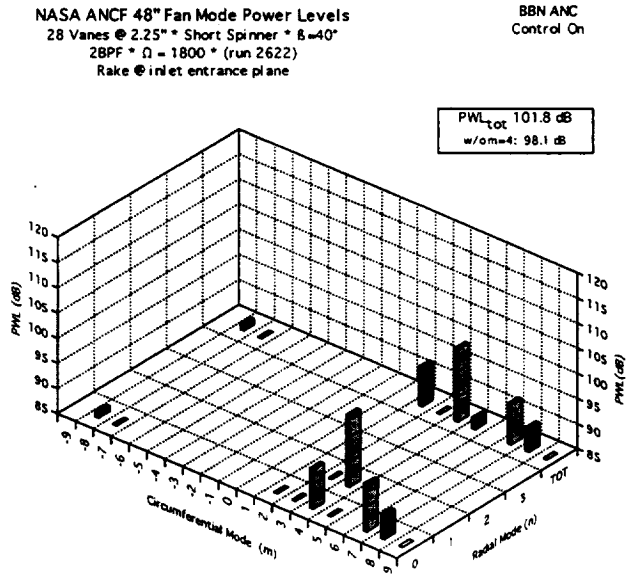

Figure 4.20: Controller mode mix at 1800 RPM

4.5 Far Field Testing

4.5.1 2BPF Tone Reduction

The 2BPF tone was the targeted fan interaction for the experiment. Far field sound pressure levels for the 2BPF tone were taken for several fan speeds from 1400 RPM to 1800 RPM. Levels were recorded with the control system on and off. This data is presented in figures 4.21 to 4.25. The results vary with speed, but reductions were observed at all of the fan speeds tested.

At 1800 RPM, the maximum SPL was reduced from 81 dB to 76 dB. In the band of peak fan interaction radiation, which occurs in a band from 40 to 80 degrees, a control reduction of between 14 dB and 5 dB is obtained. The doubling of controller gain from 0.5 to 1.0 had slight impact on performance.

At 1700 RPM the reduction in maximum SPL is modest. However, reductions of about 10 dB are obtained in a band from 20 to 40 degrees and again at the exhaust lobe at 130 degrees. The doubling of controller gain again has slight impact on performance.

At 1600 RPM maximum SPL was reduced from 76 dB to 72 dB. A broad arc of reductions of about 6 dB is obtained from 40 to 140 degrees.

At 1500 RPM the reduction in maximum SPL is from 72 dB to 66 dB. An arc of reductions of between 5 dB and 15 dB is obtained from 50 to 100 degrees.

As expected at 1400 RPM, the reduction in maximum SPL is very good from from 76 dB to 61 dB with a broad arc of reductions of over 5 dB for most of the arc of the main lobe of radiation. At this speed only one fan interaction mode can propagate in the inlet and one in the exhaust.

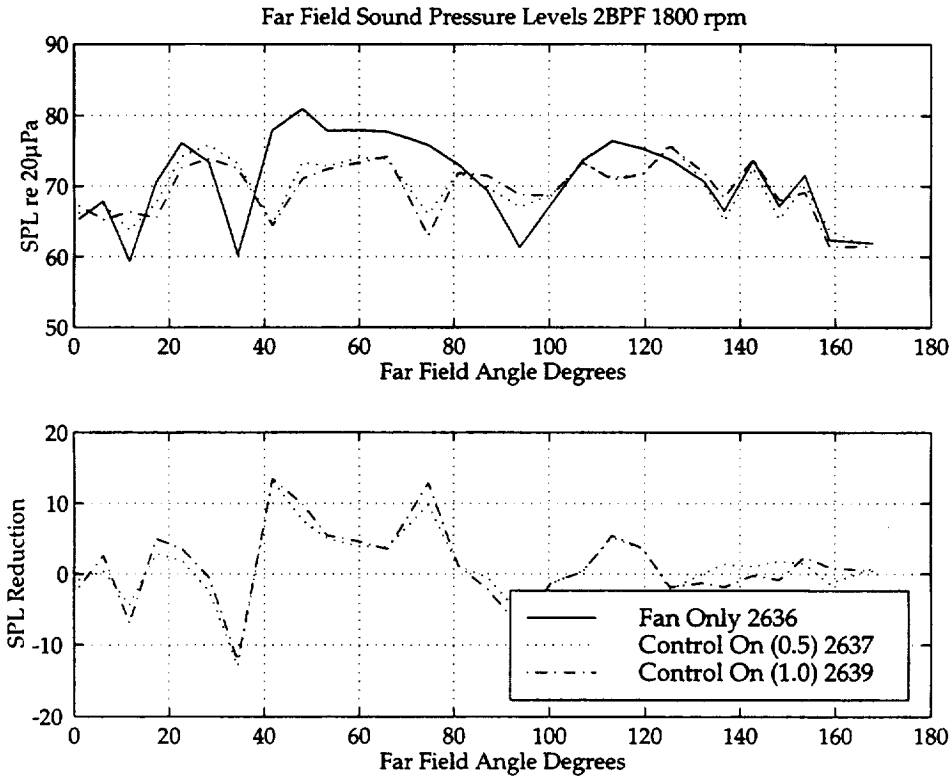

Figure 4.21: Far field sound pressure levels, 2BPF, 1800 RPM, corrected to 40 ft.

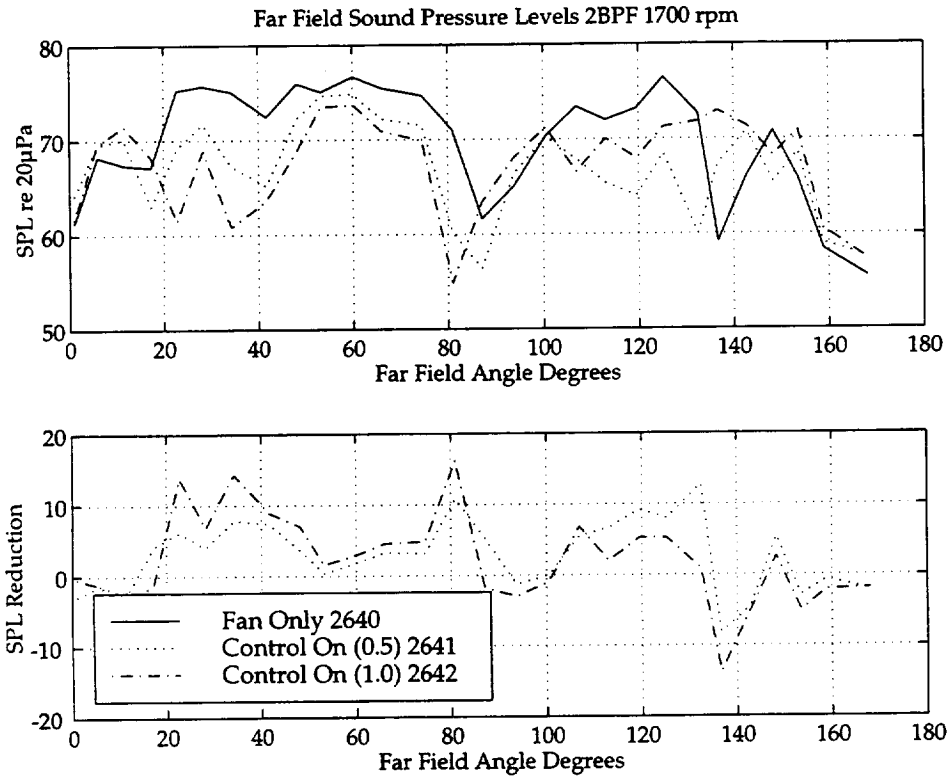

Figure 4.22: Far field sound pressure levels, 2BPF, 1700 RPM corrected to 40 ft.

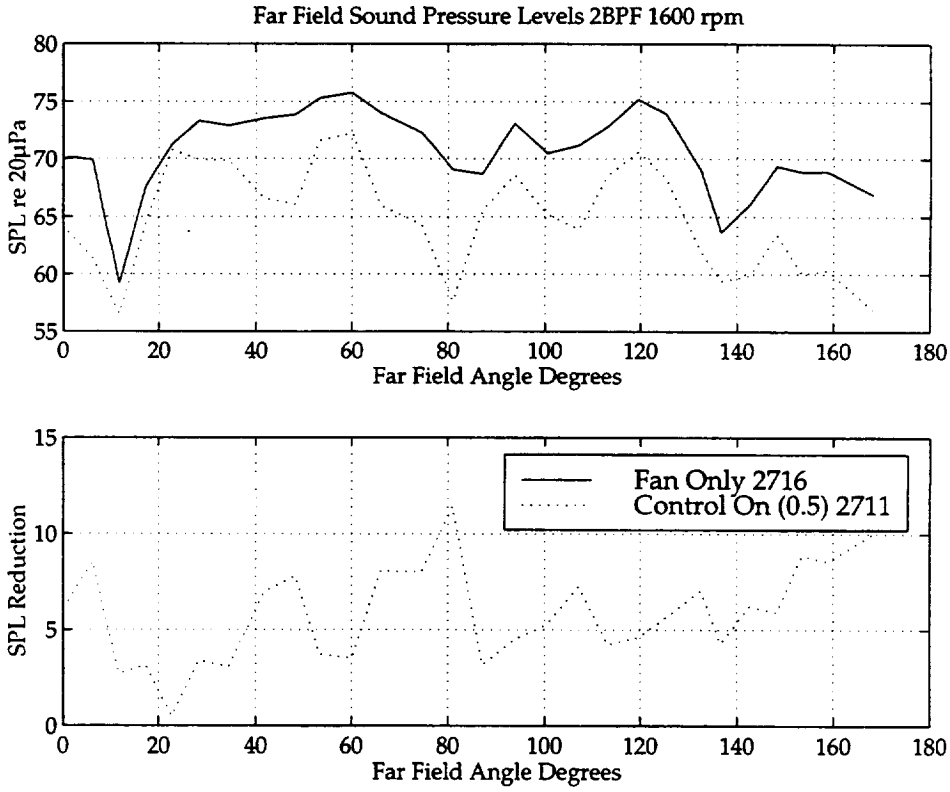

Figure 4.23: Far field sound pressure levels, 2BPF, 1600 RPM corrected to 40 ft.

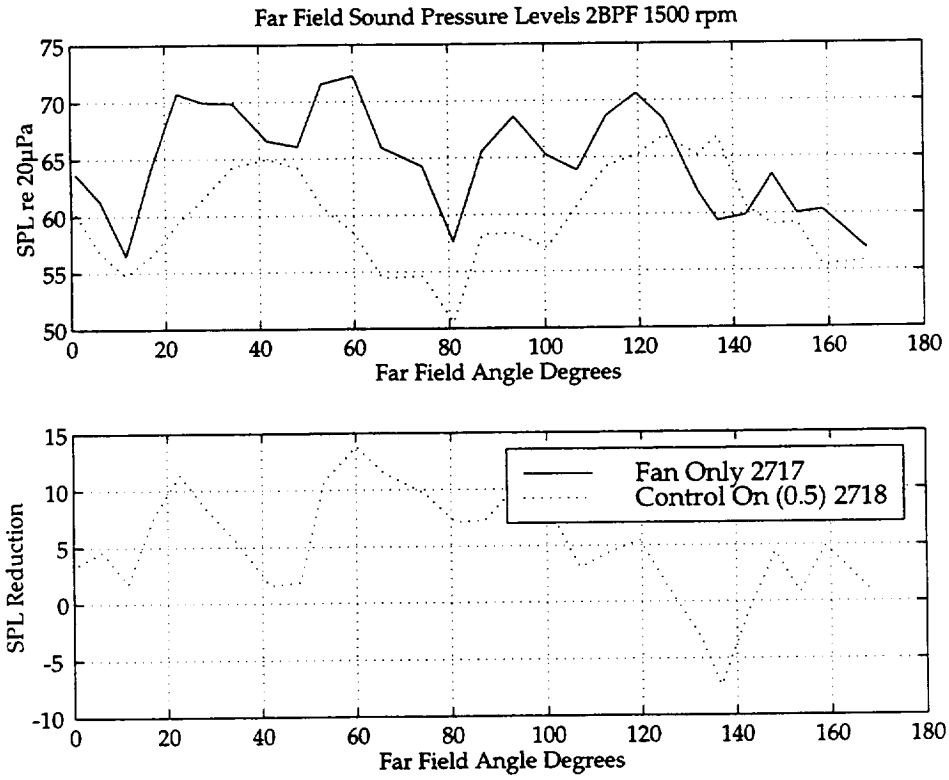

Figure 4.24: Far field sound pressure levels, 2BPF, 1500 RPM corrected to 40 ft.

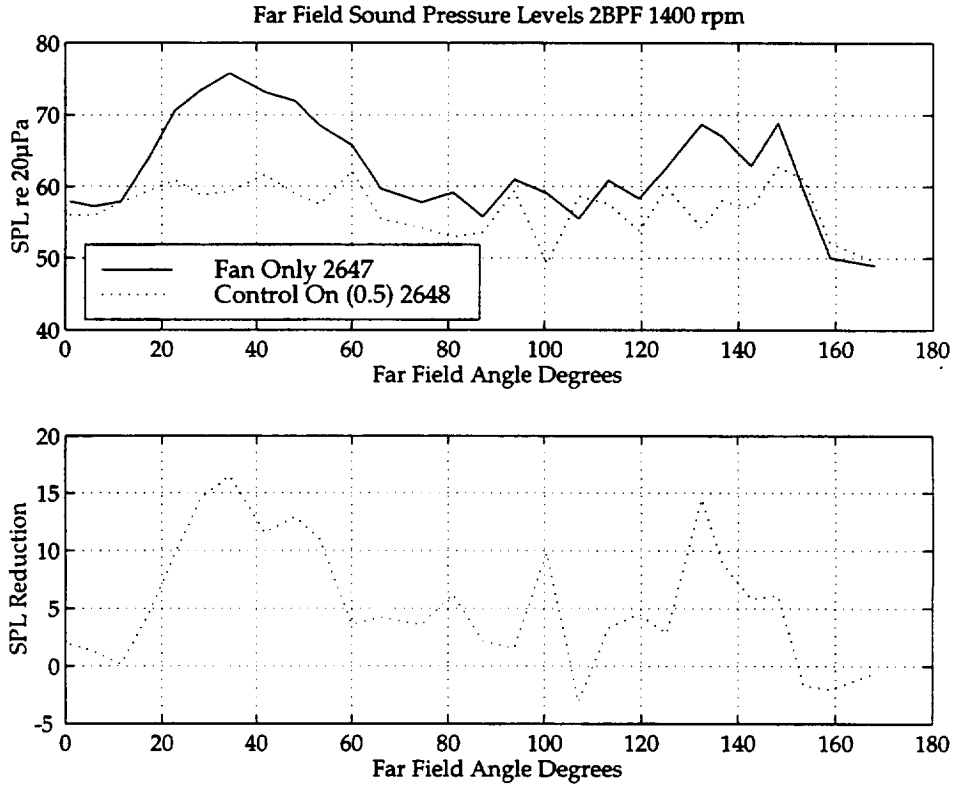

Figure 4.25: Far field sound pressure levels, 2BPF, 1400 RPM corrected to 40 ft.

4.5.2 BPF and 3BPF

A curious feature was observed when the far field sound pressure data for the BPF and 3BPF tones were analyzed. Although the control effort was exclusively directed towards controlling the 2BPF tone (BPF and 3BPF tones were filtered from the microphone signals and so the controller could know nothing of them) reductions were consistently observed in these other tones as shown in Figures 4.26 and 4.27 for a range of fan speeds.

The second explanation is that the cause is physical. The vane actuators are acting at the location of the disturbance forces. As these are caused by the fan wake being swept over the surface of the stator vane, it is possible that there is some non-linear frequency shifting effect such that reducing the major 2BPF component of the sound changes the way that a fan wake interacts with a vane. It is believed that the fan/stator interaction process is non-linear and that the vane actuators act a sources of acoustic waves and do not significantly effect the forces generated by the fan wakes or significantly reduce the effect volume deficit. However, the BPF and 3BPF data suggests that further investigations of a possible non-linear interaction between vane actuators and the physical mechanisms of fan/stator interaction may be justified.

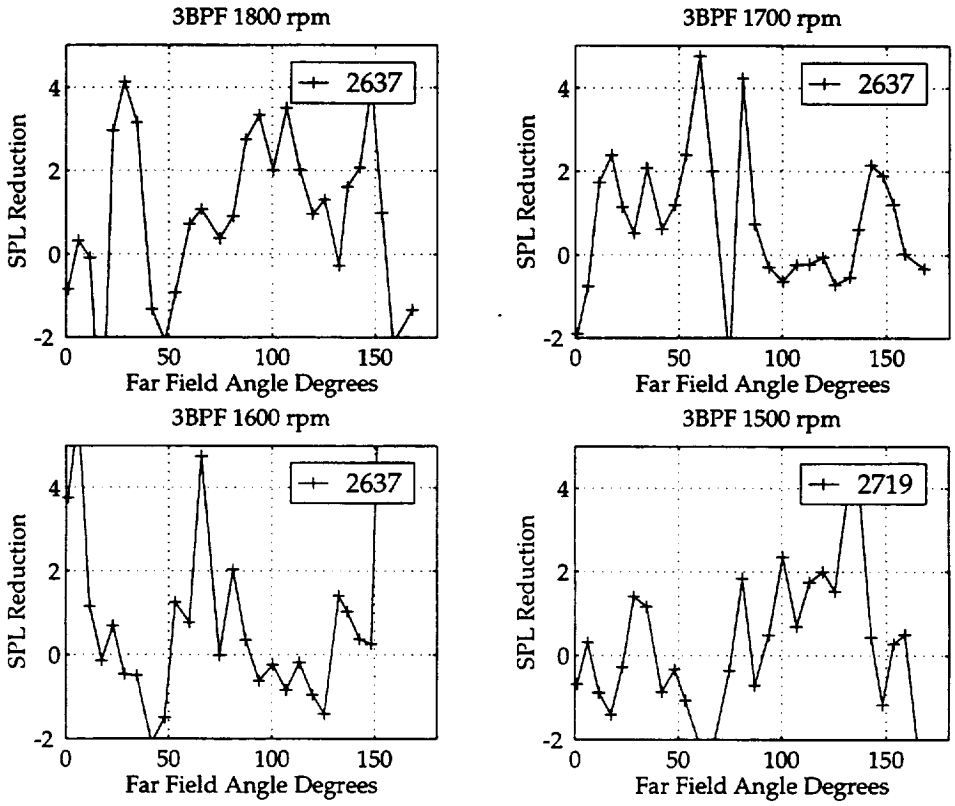

Figure 4.26: Far field sound pressure levels, BPF

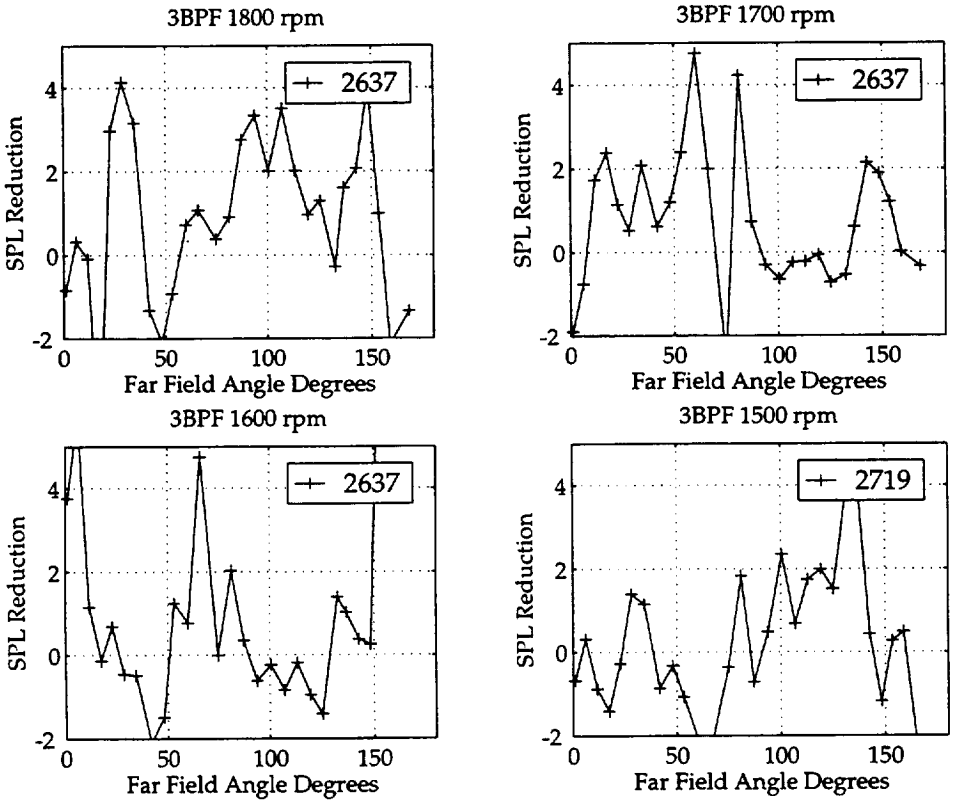

Figure 4.27: Far field sound pressure levels, 3BPF

4.5.3 Reduced System Tests

The location of the actuators on the vane places them at the same location as the disturbance source of sound, the unsteady forces on the vanes caused by the fan wakes. As both the disturbance sources and the control sources are in the same approximate location and are both dipoles, they will both couple with the duct acoustics in approximately the same way. If the actuators could be placed in exactly the right location it may be possible to simultaneously control with actuator arrays at a single axial location, the disturbance modes propagating to both inlet and exhaust.

As an experimental investigation of this effect, in duct data was taken for control systems using reduced numbers of actuator arrays. The results are summarized in Tables 4.8, 4.9 and 4.9.

The leading edge pair of actuators arrays, A1 and A3, (vane actuators #1, #2 and #3) when used alone, reduce the inlet mode power by 2.9 dB and the exhaust mode power by 5.6 dB. The trailing edge pair of actuator arrays, A2 and A4 (vane actuators #4, #5 and #6) reduce the inlet mode power by 5.8 dB and the exhaust mode power by 0.1 dB. In both cases, control of four modes by two actuator arrays has resulted in a total mode power reduction. The tip actuator arrays, A1 and A2, cannot get control of both inlet and exhaust, and although the controller indicated that there was modest reduction at the sensor arrays, there was an overall increase in total power.

The difference in performance between leading and trailing edge will be due to the different way that the actuator arrays couple with the modes, and it is interesting to note that the leading edge pair did better on exhaust modes and the trailing edge pair did better on inlet modes. Perhaps a perfectly sited pair of actuators (at mid chord?) could couple equally well with both inlet and exhaust with the correct phase to substantially reduce both mode powers. The poor performance of the tip arrays suggests that for actuators matched in location to the source, radial arrays are better than axial arrays. This would make sense if the actuators were matching the source which is effectively a distributed band of fluctuating force along the radius of the vane.

These encouraging results suggests further investigation is justified, of the effect of location of actuators on performance.

The last but one line of the tables is the performance of an array condition that simulates failure of a number of the actuators. A random sample of ten actuators were disconnected to simulate failure. The effect is expected to be a reduction in the control authority and probably more importantly an increase in modal spillover. As

expected, there was a reduction in performance, but there the controller maintained a net power reduction in both inlet and exhaust.

	Inlet			Exhaust		
Condition	(4,0)	(4,1)	m=4	(4,0)	(4,1)	m=4
Fan Only	96.9	108.6	108.9	97.7	104.4	105.3
Leading Edge	100.3	104.6	106.0	91.3	98.9	99.6
Trailing Edge	88.5	102.9	103.1	92.8	104.9	105.1
Tip Pair	104.1	108.0	109.5	101.3	104.2	106.0
Random Set	97.6	104.0	104.9	93.3	101.4	102.0
All Actuators	92.4	97.8	98.9	92.3	100.9	101.5

Table 4.8: Acoustic mode powers for the fan only and the controlled residual sound fields for reduced order control systems. Fan speed 1800 RPM

	Inlet			Exhaust		
Condition	(4,0)	(4,1)	m=4	(4,0)	(4,1)	m=4
Leading Edge	-3.4	4.0	2.9	6.4	5.5	5.6
Trailing Edge	8.5	5.7	5.8	4.9	-0.5	0.1
Tip Pair	-7.2	0.6	-0.6	-3.6	0.2	-0.8
Random Set	-0.7	4.6	4.0	4.4	3.1	3.3
All Actuators	4.5	10.8	10.0	5.2	3.5	3.8

Table 4.9: Mode powers reductions for reduced order control systems. Fan speed 1800 RPM

Chapter 5

Conclusions and Recommendations

5.1 Summary Conclusions

An active control system for ducted fan noise that uses vane actuators has been shown to be feasible. The vane actuator ANC system reduced total power levels in the target modes by up to 9 dB in the inlet and in the tone by over 6 dB while at the same time exhaust power levels were reduced by up to 3 dB.

A simplified control system with just two actuator arrays at different radial locations was demonstrated to simultaneously reduce tonal power in both inlet and exhaust.

The requirements of a vane actuator for the ANCF was a device that could be installed in a vane and produce displacements of over 0.001 of an inch at 1 kHz. An actuator based on THUNDER technology was built that met these requirements. A total of 168 actuators were installed in 28 vanes. They proved to be very robust, none of the actuators failed during the six weeks of testing. The sensitivity of the actuators was uniform across the batch; with minimal calibration control modal spillover was kept to around -10 dB.

5.2 Comments and Recommendations

The control system tested did not have sufficient control authority to reduced the level of the 2BPF tone to the level of the broadband background. The main cause

of this was the limited output of the power amplifiers. The conservative linear amplifier design used an Apex PA85 operational amplifier limited in peak output to 150 V, limiting the rms output to 100 V. The vane actuators are believed to be able to withstand maybe twice these levels. With these higher drive voltages the vane actuators would have sufficient authority to 'nail' the ANCF tones.

The level of displacement required for an engine application has been estimated to be up to 20 dB higher than that demonstrated. While admitting that this would be a challenge for the current design of actuator, there is room for improvement. Thinner PZT material than that used is available (displacement output is inversely proportional to PZT thickness with all other actuator parameters fixed). It should also be possible to improve the actuator design by more prototype experimentation with different dimensions and materials. As part of the limitation in output levels is due to inconsistencies between actuators (through the need to set the resonance frequency high and to detune an array to the performance of the weakest element), improvements in the quality of the manufacturing process will also lead to improvements output level. With this justification, and including the higher drive levels possible from an improved power amplifier design, it is reasonable to assume that a ten times increase in output is possible.

The second limitation on performance was spillover. The ability of the actuator arrays to control the fan interaction modes was reduced by the difference in sensitivity of the elements of the array. In the test only minimal calibration of the actuators was performed as exact acoustic calibration was problematic. The acoustic calibration device designed for the vane actuators proved to be difficult to use and suffered from acoustic cross talk between microphone cavities. As the performance of the system in terms of the objectives of these test was acceptable, no attempt was made to improve the calibration (this is best done on individual vanes before installation in the duct). It is reasonable to assume that some system performance would ensue from an improvements to both the manufacturing batch uniformity and to the acoustic calibration procedure.

The lack of performance in the exhaust duct did not seem to be due to lack of control authority or control spillover in the exhaust. This is certainly partly due to the lower power levels in the exhaust; a least squares control system will tend to equalize levels between inlet and exhaust. The exhaust performance maybe limited by control spillover in the inlet, which will set the floor in the least squares control cost function. As other systems, using the same sensors and vane settings, have been reported to experience similar difficulties, a plausible explanation is that the problem lies with some difficult physics of the duct. There is a cross-sectional transition that occurs just before the exit plane where the center body increases in size from a hub tip ratio of 0.35 to 0.5. The axial phase speed of the fan interaction modes will vary as they propagate through this section and perhaps they mix in some pathological

way at the exhaust sensor arrays. As real engine ducts have similar transitions in cross section, further investigation of the cause of this problem is justified.

One encouraging result was the performance of the simplified control system. A claimed strong benefit of vane actuators are that they act at the source of the disturbance. This was assumed to give some benefit in terms of efficiency. If both fan interaction and control sources are at a the same location and are both dipole sources, then they should couple with the duct acoustics in the same way. From a small and defined region, the fan interaction generates, in this case, four independent acoustic modes, two in the inlet and two in the exhaust. A correctly placed pair of control actuator arrays might couple to these four modes in a similar way, enabling two actuator arrays to control four modes. As engine applications have many fan interaction radial mode components, this efficiency of vane actuators could prove to be necessary for the practical application of ANC.

Bibliography

[1] 'Active Noise Control of Low Speed Fan Rotor-Stator Modes' D. L. Sutliff, Z. Hu, F. G. Pla, L. J. Heidelberg; AIAA-97-1641 1997.

[2] 'Active Control of Fan Noise from a Turbofan Engine'; Thomas, R.H., Burdisso, R.A., Fuller, C.R. O'Brien W.F.; AIAA Journal 1994, **32**(1) p23-30

[3] 'Active Control of Wake/Blade-Row Interaction Noise', K.A. Kousen and J.M. Verdon; AIAA 93-4351 1993.

[4] 'Actuator Feasibility Study for Active Control of Ducted Axial Fan Noise', John C. Simonich, NASA Contractor Report CR-195412, May 1995

[5] 'Aeroacoustic Analysis of Turbofan Noise Generation' Meyer, H.D. and Envia, E., NASA CR-4715, March 1996.

[6] J.M. Tyler and T.G. Sofrin 'Axial flow compressor noise studies', SAE Transactions **70** 309-332, 1962

[7] "Algorithm for multichannel LMS adpative filtering", Electronics Letters **21** 979-981 1985

[8] 'Inlet Acoustic Mode Measurements Using a Continuously Rotating Rake', Laurence J. Heidelberg and David G. Hall, Journal of Aircraft, **32**(4), p761-767, 1995.

[9] 'A Unique Ducted Fan Test Bed for Active Noise Control and Aeroacoustics Research', Laurence J. Heidelberg, David G. Hall, James E. Bridges, M. Nallasamy, NASA Technical Memorandum 107213, AIAA-96-1740, 1996

[10] 'Matrix Computations', G. H. Golub and C. F. Van Loan, The John Hopkins University Press, 1989.

[11] U.S. Patent No. 5632841 'Thin layer composite unimorph ferroelectric driver and sensor', May 27, 1997.

REPORT DOCUMENTATION PAGE

Form Approved
OMB No. 0704-0188

1. AGENCY USE ONLY (*Leave blank*)	2. REPORT DATE	3. REPORT TYPE AND DATES COVERED
	May 1999	Final Contractor Report

4. TITLE AND SUBTITLE

Active Control of Fan Noise by Vane Actuators

5. FUNDING NUMBERS

WU–538–03–11–00
NAS1–20101

6. AUTHOR(S)

Alan R.D. Curtis

7. PERFORMING ORGANIZATION NAME(S) AND ADDRESS(ES)

BBN Technologies
70 Fawcett Street
Cambridge, Massachusetts 02138

8. PERFORMING ORGANIZATION REPORT NUMBER

E–11704

9. SPONSORING/MONITORING AGENCY NAME(S) AND ADDRESS(ES)

National Aeronautics and Space Administration
John H. Glenn Research Center at Lewis Field
Cleveland, Ohio 44135–3191

10. SPONSORING/MONITORING AGENCY REPORT NUMBER

NASA CR—1999-209156

11. SUPPLEMENTARY NOTES

This report prepared for and managed by Glenn Research Center as a task of Langley Research Center Contract NAS1-20101. Project Manager, Laurence J. Heidelberg, organization code 2200, (216) 433–3859.

12a. DISTRIBUTION/AVAILABILITY STATEMENT

Unclassified - Unlimited
Subject Categories: 07 and 71 Distribution: Nonstandard

This publication is available from the NASA Center for AeroSpace Information, (301) 621–0390.

12b. DISTRIBUTION CODE

13. ABSTRACT (*Maximum 200 words*)

An active noise control system for ducted fan noise was built that uses actuators located in stator vanes. The actuators were piezoelectric benders manufactured using the THUNDER technology and were custom designed for the application. The active noise control system was installed in the NASA ANCF rig. Four actuator array with a total of 168 actuators in 28 stator vanes were used. Simultaneous reductions of acoustic power in both the inlet and exhaust duct were demonstrated for a fan disturbance that contained two radial mode orders in both inlet and exhaust. Total power levels in the target modes were reduced by up to 9 dB in the inlet and total tone levels by over 6 dB while exhaust power levels were reduced by up to 3 dB. Far field sound pressure level reductions of up to 17 dB were observed. A simpler control system, matched to the location of the disturbance with two radial actuator arrays, was demonstrated to control total acoustic power in four disturbance modes simultaneously in inlet and exhaust. The vane actuator met the requirements given for the ANCF, although in practice the performance of the system was limited by the constraints of the power amplifiers and the presence of control spillover. The vane actuators were robust. None of the 168 vane actuators failed during the tests.

14. SUBJECT TERMS

Active control fan noise; Aircraft noise; Reduction; Ducted fans

15. NUMBER OF PAGES

95

16. PRICE CODE

A05

17. SECURITY CLASSIFICATION OF REPORT	18. SECURITY CLASSIFICATION OF THIS PAGE	19. SECURITY CLASSIFICATION OF ABSTRACT	20. LIMITATION OF ABSTRACT
Unclassified	Unclassified	Unclassified	